CXCR4 Antagonism Sensitizes Cancer Cells to Novel Indole-Based MDM2/4 Inhibitors in Glioblastoma Multiforme

Simona Daniele [1,‡], Valeria La Pietra [2,‡], Rebecca Piccarducci [1], Deborah Pietrobono [1], Chiara Cavallini [1], Vincenzo Maria D'Amore [2], Linda Cerofolini [3], Stefano Giuntini [4], Pasquale Russomanno [2], Michela Puxeddu [5], Marianna Nalli [5], Martina Pedrini [6], Marco Fragai [3,4], Claudio Luchinat [3,4], Ettore Novellino [2], Sabrina Taliani [1], Giuseppe La Regina [5], Romano Silvestri [5], Claudia Martini [1,*] and Luciana Marinelli [2,*].

[1] Dipartimento di Farmacia, Università di Pisa, 56126, Pisa, Italy.

[2] Dipartimento di Farmacia, Università degli Studi di Napoli Federico II, 80131, Napoli, Italy.

[3] Magnetic Resonance Center (CERM), University of Florence, and Consorzio Interuniversitario Risonanze Magnetiche di Metalloproteine (C.I.R.M.M.P), 50019, Sesto Fiorentino (FI), Italy.

[4] Department of Chemistry "Ugo Schiff", University of Florence, 50019, Sesto Fiorentino (FI), Italy.

[5] Laboratory affiliated to Istituto Pasteur Italia – Fondazione Cenci Bolognetti - Department of Drug Chemistry and Technologies, Sapienza University of Rome, 00185, Roma, Italy.

[6] Chemistry Department, Università degli Studi di Milano, 20133, Milano, Italy.

‡ Equally contributed

* Correspondence: claudia.martini@unipi.it; Tel: +390502219522; Fax: 0502219608 (C.M.)

Abbreviations

GBM	Glioblastoma multiforme
MDM2	murine double minute 2 protein
MDM4	murine double minute 4 protein
CXCR4	C-X-C chemokine receptor type 4
GSCs	GBM stem-like cells
CSP	Chemical shift perturbation
Pmax	Maximum pressure
TLC	Thin-layer chromatography
MP	Melting points
IR	Infrared spectra
^{1}H NMR	Proton nuclear magnetic resonance
HPLC	High-pressure liquid chromatography
PDB	Protein data bank

MAX 250 WORDS

Abstract: Glioblastoma Multiforme (GBM) is a highly invasive primary brain tumor characterized by chemo- and radio-resistance and poor overall survival. GBM can present an aberrant functionality of p53, caused by the overexpression of the murine double minute 2 protein (MDM2) and its analogue MDM4, which may influence the response to conventional therapies. Moreover, tumour resistance/invasiveness has been recently attributed to an overexpression of the chemokine receptor CXCR4, identified as a pivotal mediator of glioma neovascularization. Notably, CXCR4 and MDM2-4 cooperate in promoting tumour invasion and progression. Indeed, although CXCR4 actively promotes MDM2 activation leading to p53 inactivation, MDM2-4 knockdown induces the downregulation CXCR4 gene transcription.

Our study aimed to assess if the CXCR4 signal blockade could enhance the sensitivity of glioma cells to the inhibition of the p53-MDMs axis. Rationally designed inhibitors of MDM2/4 were combined with the CXCR4 antagonist, AMD3100, in human GBM cells, and also tested in GBM stem-like cells (neurospheres), which are crucial for tumour recurrence and chemotherapy resistance. The dual MDM2/4 inhibitor RS3594 and the CXCR4 antagonist AMD3100 reduced GBM cell invasiveness and migration in single-agent treatment and mainly in combination. AMD3100 sensitized GBM cells to the anti-proliferative activity of RS3594. It is noteworthy, that these two compounds present synergic effects on cancer stem component: RS3594 inhibited the growth and formation of neurospheres, AMD3100 induced differentiation of neurospheres while enhancing RS3594 effectiveness in preventing their proliferation/clonogenicity. These results confirm that blocking CXCR4/MDM2/4 represents a valuable strategy to reduce GBM proliferation and invasiveness, acting on the stem cell component too.

Keywords: Glioblastoma Multiforme (GBM); GBM stem-like cells (GSCs); MDM2; MDM4; p53; CXCR4.

1. Introduction (MAX 500 words) Ok da rivedere numero esatto parole

Glioblastoma (GBM) represents the most common brain cancer with one of the worst survival rates (about 14 months). Due to its tremendous aggressiveness and invasiveness, the conventional therapies, including surgery, radiotherapy, and chemotherapy (temozolomide) are inefficacious, promoting its inevitable recurrence, which can be attributed mainly to the presence of self-maintaining, multipotent, tumour-initiating GBM stem-like cells (GSCs).

REF: Ostrom, Q. T.; Gittleman, H.; Farah, P.; Ondracek, A.; Chen, Y.; Wolinsky, Y.; Stroup, N. E.; Kruchko, C.; Barnholtz-Sloan, J. S. (2013) CBTRUS Statistical Report: Primary Brain and Central Nervous System Tumors Diagnosed in the United States in 2006-2010. Neuro-oncology 15 Suppl 2, ii1-56. https://doi.org/10.1093/neuonc/not151.

Van Meir, E. G.; Hadjipanayis, C. G.; Norden, A. D.; Shu, H.-K.; Wen, P. Y.; Olson, J. J. (2010) Exciting New Advances in Neuro-Oncology: The Avenue to a Cure for Malignant Glioma. CA Cancer J. Clin. 60 (3), 166–193. https://doi.org/10.3322/caac.20069.

Lim M, Xia Y, Bettegowda C, Weller M. Current state of immunotherapy for glioblastoma. Nat Rev Clin Oncol. 2018 Jul;15(7):422-442. doi: 10.1038/s41571-018-0003-5. PMID: 29643471.

Thus, GSCs represent the primary tumorigenic cells targeted by cancer therapy. Nevertheless, the GSC inherent resistance is responsible of cancer cells colonization at distant metastatic sites (Najafi et al., 2019). Thus, a stem cell-oriented treatment could represent an effective strategy, reducing ~~tumor~~tumour recurrence and improving prognosis (Liu et al., 2006).

In GBM, p53, a transcriptional regulator that integrates stress signals and induces cell cycle arrest, senescence and apoptosis (Cancer Genome Atlas Research Network, 2008), is usually aberrant and its mutations enable~~s~~ ~~tumor~~tumour cells to escape from apoptosis (Farhood et al., 2019). Moreover, the overexpression of murine double minute proteins 2 and 4 (MDM2 and MDM4) inactivates p53 by promoting its ubiquitin degradation or inhibiting its transcriptional activity, reducing the ~~tumor~~tumour suppressor functions and increasing their effectiveness by forming an MDM2/4 heterodimer. Unsurprisingly, anomalies in the p53-MDM pathway -are associated with GBM progression and more stem-like phenotype (Zhang et al., 2018).

Following the first successful compound Nutlin-3a (1, chart 1), other inhibitors able to counteract the hyperactivation of MDM proteins have been discovered.

The latest clinical trials have demonstrated a complete p53 reactivation and an effective clinical response, by targeting both MDMs simultaneously (Sestito et al., 2018). These proteins act as oncogene and invasion promoters even in a p53-independent manner, so that inhibitors may also be useful in treating p53-mutant ~~tumors~~tumours (Gao et al., 2019).

ha formattato: Colore carattere: Rosso

ha formattato: Colore carattere: Rosso

ha formattato: Colore carattere: Rosso

ha formattato: Colore carattere: Rosso

ha formattato: Colore carattere: Rosso

ha formattato: Colore carattere: Rosso

Formattato: Interlinea: 1,5 righe

ha formattato: Colore carattere: Rosso

ha formattato: Colore carattere: Rosso

ha formattato: Colore carattere: Rosso

ha formattato: Colore carattere: Rosso

ha formattato: Colore carattere: Rosso

Additionally, several data display a tight connection between the aberrant p53-MDM axis and the C-X-C chemokine receptor type 4 (CXCR4) ~~signaling~~signalling in cancers development and invasiveness.

Especially, MDM2-4 knockdown seems to significantly suppress the number of circulating ~~tumor~~tumour cells and induces a substantial downregulation of CXCR4 gene transcripts in breast cancer (Moskovits et al., 2006), whereas CXCR4 activation stimulates MDM2 expression and inhibits p53, promoting cell growth in pancreatic cancer (Arcarolli et al., 2009).

CXCR4 is overexpressed in both GBM and GSCs, thus influencing GBM malignancy, grade, and invasiveness as well as poor prognosis (Presti et al., 2018). Specifically, CXCR4 is localized in hypoxic peri-arteriolar GSC niches in GBM and plays a pivotal role in chemotherapy and irradiation resistance, maintaining GSCs in a quiescent state.

REF:Hira VVV, Breznik B, Vittori M, Loncq de Jong A, Mlakar J, Oostra RJ, Khurshed M, Molenaar RJ, Lah T, Van Noorden CJF. Similarities Between Stem Cell Niches in Glioblastoma and Bone Marrow: Rays of Hope for Novel Treatment Strategies. J Histochem Cytochem. 2020 Jan;68(1):33-57. doi: 10.1369/0022155419878416. Epub 2019 Sep 30. PMID: 31566074; PMCID: MC6931169.P

Overall, CXCR4 and MDM2/4 cooperation promotes ~~tumor~~tumour progression and invasion while their blocking leads to a complete p53 reactivation in GBM cells and GSCs.

Here, we report the identification of a potent dual MDM2/MDM4 binder (RS3594), created by modifying its indole-based precursor, previously discovered by us through a virtual screening campaign (Giustiniano et al., 2017). We demonstrated RS3594 ability to bind the p53 binding pocket of MDM2, to reactivate the p53 pathway and exhibit anti-proliferative effects on GBM cells.

To investigate the synergically action of MDMs and CXCR4 inhibitors, GBM and GSC cells were treated with RS3594 and/or AMD3100 (plerixafor, compound 2, chart 1).

The experiments revealed that both compounds reduced the invasiveness and migration of GBM cells and acted synergistically by blocking GSC proliferation and clonogenic ability.

Altogether, the results demonstrate that blocking CXCR4 and MDM2/4 could represent a valuable strategy to reduce GBM proliferation and invasiveness, acting on the stem cell component.

ha formattato: Colore carattere: Rosso

ha formattato: Colore carattere: Rosso

ha formattato: Colore carattere: Rosso

ha formattato: Colore carattere: Rosso

ha formattato: Colore carattere: Rosso

Formattato: Tabulazioni: Non a -0,76 cm

ha formattato: Colore carattere: Rosso

ha formattato: Colore carattere: Rosso

ha formattato: Colore carattere: Rosso

ha formattato: Colore carattere: Rosso

ha formattato: Colore carattere: Rosso

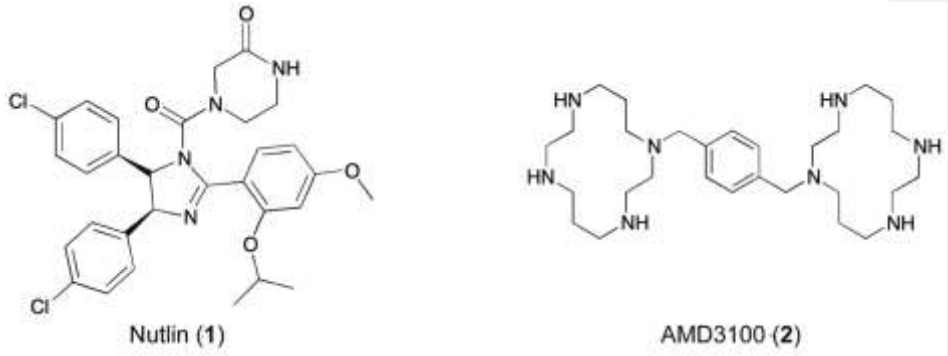

Chart 1. Chemical structures of MDM2 selective inhibitor Nutlin and CXCR4 antagonist AMD3100.

2. Materials and methods

2.1 Chemistry. All reagents and solvents were handled according to the material safety data sheet of the supplier and were used as purchased without further purification. 5-Chloro-2-methylaniline (14), 2-phenyl-1*H*-indole (17) and 2-(2-nitrophenyl)acetic acid (21) were commercially available. Microwave-assisted reactions were performed on a CEM Discover SP single-mode reactor equipped with Explorer 72 autosampler, controlling the instrument settings by PC-running CEM Synergy 1.60 software. Closed vessel experiments were carried out in capped microwave-dedicated vials (10 mL) with cylindrical stirring bar (length 8 mm, diameter 3 mm). Stirring, temperature, irradiation power, maximum pressure (Pmax), PowerMAX (simultaneous cooling-while-heating), ActiVent (simultaneous venting-while-heating), and ramp and hold times were set as indicated. The reaction temperature was monitored by an external fiber optic temperature sensor. After completion of the reaction, the mixture was cooled to 25 °C via air-jet cooling. Organic solutions were dried over anhydrous sodium sulfate. Evaporation of the solvents was carried out on a Büchi Rotavapor R-210 equipped with a Büchi V-850 vacuum controller and a Büchi V-700 vacuum pump. Column chromatography was performed using columns packed with silica gel from Merck (70−230 mesh). Silica gel thin-layer chromatography (TLC) cards from Merck (silica gel pre-coated aluminium cards with fluorescent indicator visualizable at 254 nm) were used for TLC. Developed plates were visualized with a Spectroline ENF 260C/FE UV apparatus. Melting points (mp) were determined on a Stuart Scientific SMP1 apparatus and are uncorrected. Infrared spectra (IR) were recorded on a PerkinElmer Spectrum 100 FT-IR spectrophotometer equipped with universal attenuated total reflectance accessory. IR data were acquired and processed by PerkinElmer Spectrum 10.03.00.0069 software. Band position and absorption ranges are given in cm^{-1}. Proton nuclear magnetic resonance (^1H NMR) spectra were recorded with a Bruker Avance (400 MHz) spectrometer in the indicated solvent. Fid files were processed by MestreLab

Research SL MestreReNova 6.2.1-769 software. Chemical shifts are expressed in ppm from tetramethylsilane. The purity of biologically evaluated compounds was found to be >95% by high-pressure liquid chromatography (HPLC). Thermo Fisher Scientific Inc. Dionex UltiMate 3000 HPLC system consisted of an SR-3000 solvent rack, an LPG-3400SD quaternary analytical pump, a TCC-3000SD column compartment, a DAD-3000 diode array detector, and an analytical manual injection valve with a 20 µL loop. Samples were dissolved in acetonitrile (1 mg mL^{-1}). HPLC analysis was performed by using a Thermo Fisher Scientific Inc. Acclaim 120 C18 column (5 µm, 4.6 mm × 250 mm), at 25 ± 1 °C with an appropriate solvent gradient (acetonitrile/water), flow rate of 1.0 mL min^{-1} and signal detector at 206, 230, 254, and 365 nm. Chromatographic data were acquired and processed by Thermo Fisher Scientific Inc. Chromeleon 6.80 SR15 Build 4656 software. Compounds 3-11 and RS3594 were prepared as previously reported (see supporting information).

2-(1-(Phenylsulfonyl)-1H-pyrrol-3-yl)-3-((3,4,5-trimethoxyphenyl)thio)-1H-indole (12). To a suspension of sodium hydride (0.044 g, 1.0 mmol; 60% suspension in mineral oil) in anhydrous *N,N*-dimethylformamide (2 mL) was added 23 (0.150 g, 0.46 mmol) and the resulting mixture was stirred for 10 min at 25 °C. bis(3,4,5-Trimethoxyphenyl)disulfide (0.200 g; 0.5 mmol) was added and the mixture was placed in the microwave cavity (closed vessel mode, PMax = 200 psi). Starting microwave irradiation of 150 W was used, the temperature was ramped from 25 °C to 110 °C, while stirring actively. Once 110 °C was reached, taking about 1 min, the reaction mixture was held at this temperature for 2 min. The reaction mixture was diluted with water and extracted with ethyl acetate. The organic layer was washed with brine, dried and filtered. Evaporation of the solvent gave a residue that was purified by column chromatography (silica gel, *n*-hexane: acetone = 7:3) to give 12 (0.032 g, 13%), mp 67-69 °C (from ethanol). ^{1}H NMR (DMSO-d_6): δ 3.46 (s, 6H), 3.55 (s, 3H), 6.29 (s, 2H), 7.07-7.10 (m, 2H), 7.17 (t, J = 7.0 Hz, 1H), 7.41-7.49 (m, 3H), 7.58-7.63 (m, 2H), 7.72-7.75 (m, 1H), 7.88-7.90 (m, 2H), 7.96-7.97 (m, 1H), 11.90 ppm (br s, disappeared after treatment with D_2O, 1H). IR: ν 3285 cm^{-1}.

Detailed chemical syntheses have been described elsewhere (Hugon et al., 2003; La Regina et al., 2015, 2013, 2011; Liu et al., 2014) and can be found in the Supplementary Materials.

2.2 Molecular Modeling

The ligand tridimensional structures were generated with the Maestro Build Panel and prepared using Ligprep considering all their tautomeric and protonation states at physiological pH (7.4 ± 1.5) (Greenwood et al., 2010; Shelley et al., 2007).

As concerning the protein X-ray selection, multiple 3D X-ray structures of both MDM2 and MDM4 can be found in the Protein Data Bank (PDB). Among them, we took into consideration only the ones human or humanized ones containing the N-terminus residues. Among these, the structures with the highest resolution were chosen for our docking calculations: PDB 3LBL for MDM2 and PDB 4N5T for

MDM4. In particular, the latter protein is a humanized zebrafish MDM4, where the two mutations L46V/V95L were generated by DNA site-directed mutagenesis whereas the additional E20Q modification was manually produced in order to make the whole cavity of 4N5T, including the N-terminus region, identical to that of a human MDM4.

The two receptors were prepared using the Protein Preparation Wizard implemented in Maestro Suite (Schrödinger Release 2019-2: Schrödinger Suite 2019-1) (Friesner et al., 2006, 2004; Halgren et al., 2004). During the preparation, all water molecules were deleted, hydrogen atoms added, and the complex minimized. The search areas were identified through the grid generation tool in Glide 6.7 (Friesner et al., 2006, 2004; Halgren et al., 2004) and centered around the crystallized ligand using default settings. The OPLS3E force field was employed for docking. The results of the calculations were evaluated and ranked based on the Glide XP scoring function. Thus, the top-ranked compounds were visually inspected for their binding modes and good chemical geometry. The selected poses, in the two proteins, for the most active compound RS3594, were then optimized through 20000 steps of energy minimization. The ligand-receptor complexes were solvated in a 12.0 Å layer cubic water box using the TIP3P water model parameters (Jorgensen et al., 1983). 4 Cl^- anions were used to neutralize the system. The ff14SB (Maier et al., 2015) and gaff Amber force fields (Wang et al., 2004) were used to parameterize the protein and ligand, respectively. Amber charges were applied to the proteins and water molecules, whereas ligand charges were computed using the AM1-BCC charge model (Jakalian et al., 2002). Harmonic constraints were employed and gradually released along the minimization process using the NAMD 2.9 code (Phillips et al., 2005).

2.3 Cell lines, cell culture, and neurosphere isolation. The U87MG, T98G, and U343MG cell lines were obtained from the National Institute for Cancer Research of Genoa (Italy), American Type Culture Collection (USA) and Cell Lines Service GmbH (Germany), respectively, and were cultured as previously described (Daniele et al., 2015a, 2014a). The human breast cancer cell line MCF-7 (kindly provided by Prof. Alessandra Braca, University of Pisa, Italy) was cultured in DMEM/F-12 supplemented with 10% FBS, 2mM L-glutamine, 100 U mL^{-1} Penicillin, 100 mg mL^{-1} Streptomycin at 37 °C in 5% CO_2. The immortalized human microglial C20 cells (kindly donated by Prof. Cristian Wetzel, University of Regensburg, Germany) were maintained in DMEM/F-12 supplemented with 10% FBS, 100 U mL^{-1} Penicillin, 100 mg mL^{-1} Streptomycin and 600 µg mL^{-1} of Neomycin at 37 °C in 5% CO_2. Each cell line was monitored for DNA profiling. The cells were used within low passages after their thawing.

To isolate neurospheres, U87MG cells (approximately 2 x 10^6 cells) were suspended in Neural Stem Cell (NSC) medium (DMEM/F-12 supplemented with 20 ng mL^{-1} of basic fibroblast growth factor, 20 ng mL^{-1} of epidermal growth factor and 20 ng mL^{-1} of B27 supplement) and maintained at

37 °C in 5% CO_2 for 5-7 days to allow the formation of the neurospheres. The detached neurospheres were collected and seeded for the experiments.

2.4 Dissociation studies of native MDM2/p53 and MDM4/p53 complexes. To test the ability of the compounds 3-13 to disrupt MDM2/p53 and MDM4/p53 interactions, a quantitative immunoenzymatic assay was performed on cell lysates obtained from U87MG cells (for p53/MDM2) or SHSY-5Y (for p53/MDM4) (Daniele et al., 2016, 2014a). In brief, wells were precoated with full-length anti-MDM2 (sc-965, Santa Cruz Biotechnologies) or anti-MDM4 (sc-74468, Santa Cruz Biotechnologies) antibody overnight at room temperature. U87MG or SHSY-5Y cells were suspended in lysis buffer (20 mM Tris HCl, 137 mM NaCl, 10% glycerol, 1% NONIDET40, 2 mM EDTA, pH 8) containing 1% of the Protease inhibitor Cocktail (SigmaAldrich, Milan, Italy), treated with different concentrations of compounds for 10 minutes at room temperature and then transferred to the precoated wells for 90 minutes. After extensive washes, each well was incubated with 1% BSA to block nonspecific sites, and then treated for 90 minutes with an anti-p53 antibody (70R-31561, Fitzgerald). Then, wells were washed and treated with an anti-rabbit HRP conjugated antibody. The TMB substrate kit (Thermo Fisher Scientific) permitted the colorimetric quantification of the complexes. Absorbance was measured at 450 nm. Dose−response curves were derived with Graph Pad Prism 6 software, from which IC_{50} values were obtained.

2.5 Western blotting analysis. Proteins were quantified with the Bradford assay. A total amount of 30 μg of proteins per each sample was separated onto a pre-cast 4-20% polyacrylamide gel (Mini-PROTEAN® TGX gel, Biorad) and transferred to PVDF membranes (Trans-Blot® TurboTM PVDF Transfer packs, Biorad). The membranes were blocked with 5% BSA diluted in Tris-buffered saline (TBS, 20 mM Tris-HCl, 150 mM NaCl, pH 7.5) with 0.1% Tween 20. Primary antibodies against GAPDH (G9545, Sigma-Aldrich, diluted 1:5000) and p53 (70R-31561, Fitzgerald, diluted 1:500) were used (Daniele et al., 2015a, 2014a). Protein bands were detected with ECL reagents (Clarity™ Western ECL Blotting Substrate, Biorad). Densitometry was performed by ImageJ Software.

2.6 RNA extraction and Real-Time RT-PCR analysis. U87MG were treated with AMD3100 (10 μM) and RS3594 (1 μM), alone or in combination for 24 h. Following treatments, cells were collected, and total RNA was extracted using the RNeasy Mini Kit (Qiagen, Hilden, Germany). cDNA synthesis was performed with 500 ng of RNA (BioRad, Hercules, USA). The expression levels of MDM2 were evaluated by quantitative Real-Time RT-PCR using Fluocycle II SYBR (Euroclone, Milan, Italy).

Primer sequences, annealing temperatures, and product sizes have been described elsewhere (Daniele et al., 2015b).

2.7 Cell proliferation assay. U87MG, U343MG, T98G, MCF-7, or C20 cells were plated into a 96-well plate (3 x 10^3 cells/well) in the respective culture medium. 24 h after seeding, cells were treated with AMD3100 and RS3594 alone or in combination, at the indicated concentrations. Following 72 h of incubation, the medium was replaced with fresh medium and the viability was assessed by the MTS assay (CellTiter 96 AQueous One Solution Cell Proliferation Assay kit; Promega), according to the manufacturer's instructions.

Neurospheres were collected, dissociated into single cells, and seeded into a 24-well plate (6 x 10^4 cells/well) in fresh NSC medium containing AMD3100 and RS3594 alone or in combination at the indicated concentrations. Following 7 days, viability was assessed by MTS assay, as previously described (Daniele et al., 2014b). The number and area of formed neurospheres in response to the various treatments, as well as the length of the cellular process, were quantified, as previously described (Daniele et al., 2015b).

2.8 Measurement of cell migration. RS3594 and AMD3100 effects on U87MG cell migration were evaluated with a scratch assay (Sestito et al., 2016). U87MG were seeded in 24 well plates at a density of 1x10^4 cells/wells. Then, the scratch was made through the cell layer using a sterile micropipette tip. After washing with PBS, cells were treated with RS3594 and AMD3100 in medium with 1% of FBS, alone or in combination at the indicated concentrations. The images of the wounded area were captured immediately after the scratch (t0), 8 h (t8), and 24 h later (t24) to monitor cell migration into the wounded area. Photographs were then taken at 4X magnification on an inverted microscope. The migration abilities were quantified by measuring both the average gap width and the percentage of gap closed. The data were analyzed with ImageJ Software.

2.9 Measurement of cell invasiveness. The effect of RS3594 and AMD3100 on cell invasion through Matrigel was assessed using U87MG cells. Briefly, the surface of each transwell was coated with Matrigel basement membrane matrix (BD Bioscience) (0.32 mg mL^{-1}) and incubated at 37 °C overnight to allow the proteins to polymerize, as described (Nuti et al., 2011). U87MG (5 x 10^4 cell/200 µL) were suspended in non-complete medium, treated with RS3594 and AMD3100, alone or in combination at the indicated concentrations, and added to the upper compartment of each transwell. In parallel, 500 µL of EMEM containing 10% FBS was placed in the lower compartment of each transwell. Transwells were incubated at 37 °C for 24 h; then, the non-migrating cells were removed through a

cotton bud, while the invading cells on the lower surface of the transwell were fixed with p-formaldehyde and stained with crystal violet. Pictures of casually selected light microscope fields were acquired (three fields for each filter) and the number of the invading cells was quantified through ImageJ Software (Gabelloni et al., 2010; Nuti et al., 2011).

2.10 Clonogenic assay. To assess the clonogenic potential of U87MG cells, neurospheres were dissociated with trypsin/EDTA and seeded in a 96-well plate in NSC medium at a density of 1, 5, 10, 50 and 100 cells, in the presence of RS3594 and AMD3100 alone or in combination at the indicated concentrations. Following 7 days of treatment, microscopic images of each well were acquired and the neurospheres were counted using ImageJ Software.

2.11 Cellular Apoptosis in U87MG Cells. U87MG cells were treated with RS3594 (1 µM) and AMD3100 (10 µM), alone or in combination, for 48 h. Living, apoptotic, and dead cells were acquired and ~~analyzed~~analysed by Muse Cell Analyzer. (Daniele S, Pietrobono D, Costa B, et al. Bax Activation Blocks Self-Renewal and Induces Apoptosis of Human Glioblastoma Stem Cells. ACS Chem Neurosci. 2018 Jan 17;9(1):85-99. doi: 10.1021/acschemneuro.7b00023).

ha formattato: Evidenziato

2.12 Statistical analyses. Graph-Pad Prism (GraphPad Software Inc., San Diego, CA) was used for data analysis and graphic presentations. Statistical analyses were achieved through a one-way ANOVA study followed by the Bonferroni test for repeated measurements. All data are shown as the mean ± SD. Differences were considered statistically significant with $p<0.05$ (Daniele et al., 2017a).

2.13 NMR measurements

The MDM2 protein used for NMR studies was cloned, expressed, and purified as previously described (Giustiniano et al., 2017; Merlino et al., 2018). All the spectra were acquired at 298 K on a Bruker AvanceNEO NMR spectrometer operating at 700 MHz ^{1}H Larmor frequency, equipped with a cryogenically cooled probe optimized for ^{13}C sensitivity (TCI, S/N 1500:1, on the ASTM standard sample) as well as for ^{1}H sensitivity. The spectra were processed with the Bruker TOPSPIN software packages and analyzed by the program Computer Aided Resonance Assignment (ETH Zurich; Keller, 2004).

The protein assignment was based on the data reported in the Biological Magnetic Resonance Data Bank under the accession code 6612 (Uhrinova et al., 2005). During the NMR titration of the protein with RS3594, aliquots of a DMSO-d6 solution of the compound (100, 200, 400, 800 µM) were added

to the buffered solution (50 mM KH_2PO_4, 50 mM Na_2HPO_4, pH 7.5, 150 mM NaCl) of the ^{15}N isotopically enriched MDM2 protein at the concentration of 200 μM. 2D ^{1}H–^{15}N HSQC NMR spectra were recorded during the titration after each addition of the ligand.

3. Results

3.1 Design and Chemistry. In our previous work (Giustiniano et al., 2017) a Virtual Screening campaign was sequentially carried out on the crystal structures of MDM2 (PDB 3LBL) (Popowicz et al., 2010) and MDM4 (PDB 4N5T) (Chang et al., 2013) by using our in-house database. One of the molecules selected, a 2-phenylindole molecule (RS3760, here named 3, see Table 1) was found to be capable of disrupting the MDM2/p53 complex with an IC_{50} in a high nanomolar range (270 nM) and was less effective on the MDM4/p53 complex (% disruption 54% at 100 μM, IC_{50} >1000 nM). Taking into account that many analogs of derivative 3 were already available in our chemical library, we proved the inhibitory activity of the same selected on the base of the docking poses of 3 on MDM2/MDM4 showed in Fig. 1. Actually, besides several close analogs of 3 (4-9), also longer molecules endowed with a sulfonyl-phenyl branch (10-13) were selected from our database for binding assays in the attempt to reach the N-terminus region (see Fig. 1 and SI for synthesis details). In fact, in our experience, an extensive occupancy of the binding site, including the Leu26 subpocket and/or the N-terminus region, is important to reach a high affinity toward the MDM proteins (Merlino et al., 2018).

Commentato [RP1]: Modificare il titolo del paragrafo "more informative" (rev3)

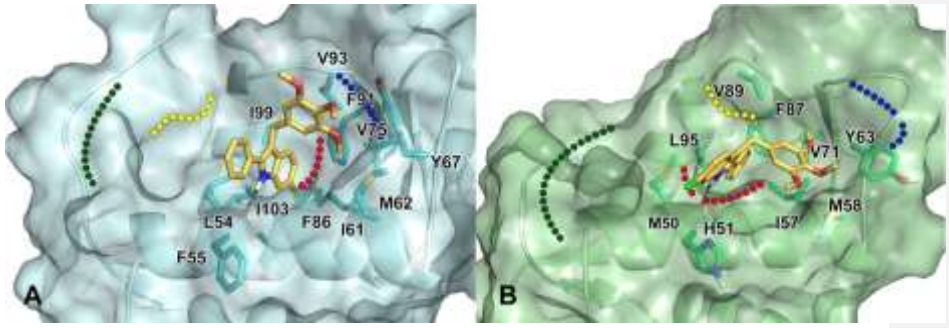

Fig. 1. **Theoretical Binding Mode of Compound 3.** Docking poses of compound **3** in MDM2 (A) and MDM4 (B) binding cavity. The ligand is shown as golden sticks, while the proteins are depicted as transparent cyano and green surfaces, with the interacting residues highlighted as cyan and light-green sticks, for MDM2 and MDM4 respectively. For the sake of clarity, the MDMs binding subpockets are depicted as blue (Phe19), red (Trp23), yellow (Leu26), and green (N-terminus) dots, in accordance with the p53 interacting side chains.

Table 1. Effect of new compounds on the dissociation of human p53/MDMs complex.

Compound	IC_{50}[1] (nM) MDM2/p53	IC_{50}[2] (nM) MDM4/p53
RS3760 (3) 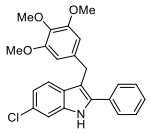	270 ± 31	>1000
RS3952 (4) 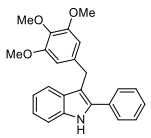	421 ± 40	503 ± 49
RS3174 (5) 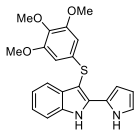	311 ± 36	547 ± 58
RS3544 (6) 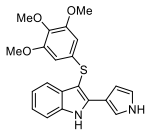	193 ± 16	255 ± 28
RS3596 (7) 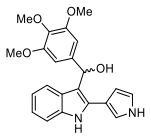	85.6 ± 8.6	42.6 ± 3.6
RS3600 (8)	201 ± 19	559 ± 56

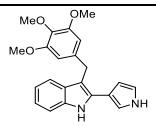		
RS3925 (9)		
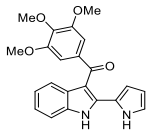	591 ± 57	>1000
RS3559 (10)		
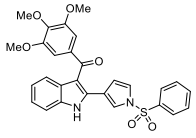	97.3 ± 9.6	212 ± 19
RS3593 (11)		
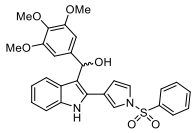	222 ± 25	238± 29
RS6001 (12)		
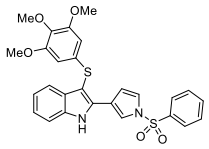	73.6 ± 6.9	76.5 ± 25
RS3594 (13)		
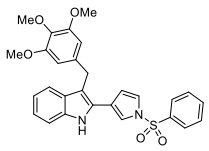	10.6 ± 1.5	18.3 ± 2.1

The name, the structure, and the IC_{50} of each compound are shown in the Table. Data represent the mean values (±SEM) of three independent determinations.[1]Concentration (nM) leading to half-maximal

inhibition of p53/MDM2 complex.[2]Concentration (nM) leading to half-maximal inhibition of the p53/MDM4 complex.

3.2 Dissociation studies: RS3594 affinity to MDM2/p53 and MDM4/p53 complexes. The ability of compounds 3-12 and RS3594 to dissociate p53 from MDM2 and MDM4 was analyzed with an immunoenzymatic assay using cell lysates obtained from U87MG and SHSY-5Y, respectively, expressing high levels of the p53-MDM2 and p53-MDM4 complexes (Daniele et al., 2016, 2014a). The standard MDM2 ligand (Nutlin-1) and the standard MDM4 ligand (SJ-1722550) were tested in parallel experiments. Dose−response curves were derived with Graph Pad Prism 6 software (data not shown), from which IC_{50} values were obtained and reported in Table 1.

All the tested compounds were able to bind MDM2 in the nanomolar range in U87MG cell lysates. In particular, compounds 3-6 showed moderate affinity, in the medium-high nanomolar range. Similar results were obtained with compounds 8, 9, and 11. In contrast, compounds 7, 10, and 12 displayed a good ability to bind MDM2, with IC_{50} values below 100 nM. Compound RS3594 showed the highest affinity, with an IC_{50} value of 10 nM (see Table 1).

In general, the ability of compounds to bind MDM4 was lower compared to MDM2. Nevertheless, all the tested compounds, except 3 and 9, showed a moderate affinity towards MDM4, demonstrating that they can act as dual MDM2-4 ligands. In particular, compounds 7, 12, and RS3594 showed a good affinity to MDM4, with IC_{50} values lesser than 100 nM. Among these compounds, the compound RS3594 showed the highest ability to bind both MDM2-4 proteins. All the remaining molecules, i.e., compounds 4-6, 8, and 10-11 demonstrated IC_{50} values in the medium-high nanomolar range (see Table 1).

3.3 NMR and Computational Studies: identification of the Binding Site and Binding mode of RS3594 on MDM2. The binding of RS3594 to MDM2 protein was evaluated by solution NMR. Increasing aliquots of RS3594 (in order to obtain nominal concentrations of 100, 200, 400 and 800 μM, respectively) have been added to a buffered solution (50 mM KH_2PO_4, 50 mM Na_2HPO_4, 150 mM NaCl, at pH 7.5) of the protein at the concentration of 200 μM. The MDM2 amino acids forming the binding site for RS3594 have been identified by monitoring the intensity decreases of NMR signals and the chemical shift perturbations by means of 2D $^{1}H–^{15}N$ HSQC NMR spectra collected for the free protein and for the protein in the presence of the ligand. Particularly, the residues T10, Y56, L57, G58, Q59, I61, M62, D68, V75, Y76, V93, H96, Y100 displayed the highest intensity decreases (Fig. 2A), while I19, D46, F55, G58, Q59, M62, H73, C77, D84, F91, S92, H96 exhibited the highest chemical shift perturbations (CSP, Fig. 2B).

Mapping the residues exhibiting the largest chemical shift perturbation and those that exhibit a decrease in the intensity on the MDM2 structure, it is clear that RS3594 binds the canonical site of the protein. In fact, all these residues are located on the α2 helix, L2 and L5 loops, and β1 and β2 strands, which are all segments lining the p53-binding cavity (Fig. 2C).

However, during the titration, precipitation of RS3594 has been observed. This prevents an exact estimation of the ligand concentration in the protein buffered solution and in turn of its affinity.

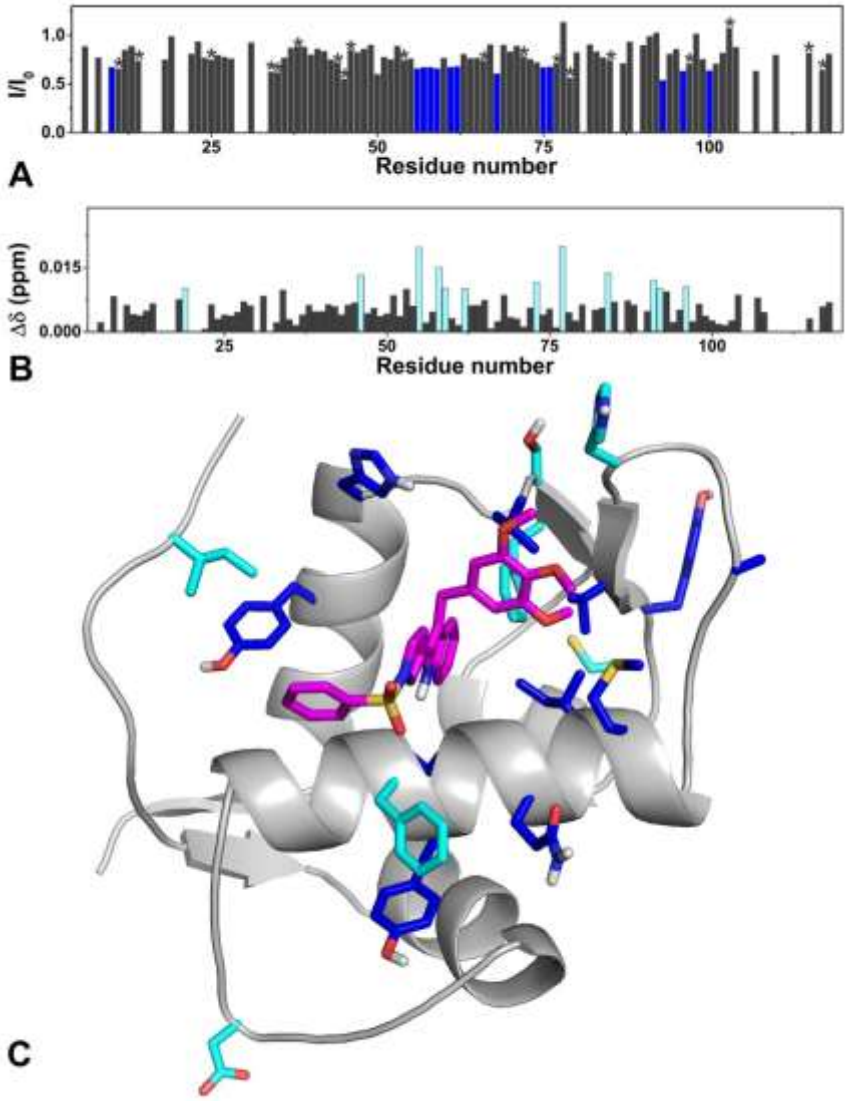

Fig. 2. Intensity decreases of NMR signals and the chemical shift perturbations. (A) Residues exhibiting the highest intensity decreases are highlighted in blue. The overlapping signals have been marked with a star and not considered in the selection. (B) Residues exhibiting the highest CSP, are highlighted in cyan and evaluated according to the formula:

Commentato [F2]: Manca legenda della figura C

$$\Delta\delta = 1/2\sqrt{(\Delta\delta_H)^2 + \left(\Delta\delta_N/5\right)^2}$$

The data reported in Fig. 2A and 2B were collected from the experiments carried out by adding RS3594 to the protein solution in order to have a nominal concentration of 400 μM of the ligand (C) CSP mapping on the structure of the protein (PDB 3LBL) in the presence of RS3594 resulting from docking; the residues with the highest intensity decreases are in blue, the ones with the largest perturbation are highlighted in cyan, while RS3594 is in magenta.

As suggested by NMR data RS3594 was docked into the canonical binding site of MDM2 and as estimated via by Glide 7.6 software, analogically to MDM4, and then the obtained complexes were minimized. As shown in Fig. 3A and B, in our docking predictions RS3594 binds the two MDMs in the same fashion. In particular: the indole scaffold plunges into the Trp23 pockets (interacting residues in MDM2: L54, F86, F91, I99, I103; in MDM4: M50, F87, V89, L95) H-bonding the L54 and the M50 backbone respectively, while the trimethoxy-phenyl ring occupies the Phe19 sites (interacting residues in MDM2: I61, M62, Y67, V75, V93; in MDM4: I57, M58, Y63, V71). In MDM2 then, the pyrrole ring in position 2 is oriented toward the Phe55 residue and the sulfonyl-phenyl moiety stretches along the α2 helix and, thanks to the considerable bending, almost reaches the internal cavity of the N-terminus region where hydrophobic contacts are established with the Q24 side chain and the K41 carbon atoms. Also, a slight movement of the flexible K41 side chain could allow the formation of a cation-pi interaction. In MDM4, the phenyl-sulfonamide moiety is oriented exactly in the same way as in MDM2, but in this protein, the K57 (corresponding to the MDM2 K41) is already well placed to form a strong cation-pi interaction.

Noteworthy, this theoretical binding mode would be in line with the above-presented NMR data. In fact, in Fig. 2C, where the described docking pose of RS3594 in MDM2 is visible, the ligand is surrounded by the residues exhibiting the largest CSP and the highest intensity decrease.

The selected poses also justify the low nanomolar IC_{50} of RS3594 toward MDMs and are in line with the other experimental IC_{50}s listed in Table 1. In fact, looking at the activity of compounds 10, 12 and RS3594, as predicted, it is evident that a broader aromatic moiety allows a better occupancy of the binding clefts in both MDMs and confers lower IC_{50} values with respect to their smaller precursors 5, 6, 8 and 9. Moreover, it appears that the flexibility of the linker connecting the indole scaffold with the trimethoxy-phenyl moiety also affects the binding affinities (see Table 1). For example, compound 9 endowed with a very rigid carbonyl linker, is the less active derivative of the small pyrrole series, while its more conformationally free analogs 5, 6 (sulfur), 7 and 8 (methylene) are more active. This different ability in ligand accommodation is observed also when the sulfonyl-phenyl branch is introduced. In fact, the longer derivatives 10 (carbonyl linker, low flexibility), 12 (sulfur linker, medium flexibility) and RS3594 (methylene linker, high flexibility), possess decreasing IC_{50} values (97 nM, 73 nM, 10 nM on

MDM2; 212 nM, 76 nM, 18 nM on MDM4, respectively). Notably, compound 11 is the only one that deviates from this trend. Although it possesses a fair flexible linker, docking calculations show that the steric hindrance of the linker hydroxyl group hampers the proper accommodation of the trimethoxy-phenyl group into the Phe19 subpocket, which is consistent with its high IC_{50} value.

Crucially, RS3594 was predicted to cross the blood-brain barrier (Table S1 and Fig. S1) (Liu et al., 2014).

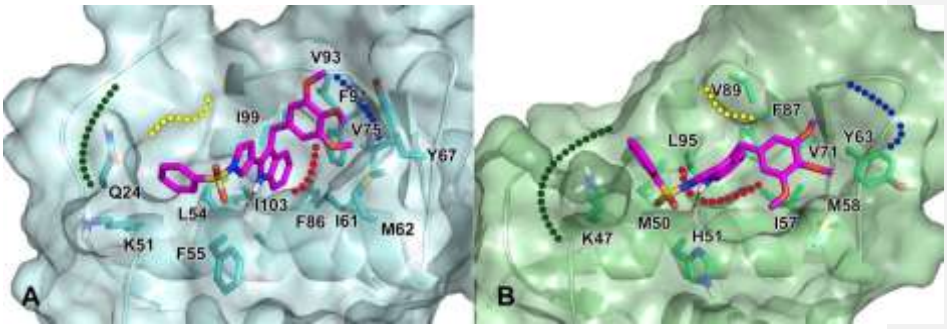

Fig. 3. **Docking results obtained for compound RS3594.** The complex of RS3594 in MDM2 (A) and MDM4 (B) binding sites, as obtained after minimization. The ligand is shown as magenta sticks, the protein surface as transparent cyan (MDM2) and transparent pale-green (MDM4), while the interacting residues as cyano and green sticks, respectively.

3.4 Reactivation of the p53 pathway by RS3594 in GBM cells. In order to verify that the most active compound RS3594 was able to restore the p53-MDMs axis, p53 protein accumulation was verified with GBM cell treatment. To this purpose, the IV grade-astrocytoma cell line, U87MG, was chosen as an appropriate cellular model expressing a wild-type p53 and CXCR4 (Hira et al., 2017; Nimmagadda et al., 2009; Zagzag et al., 2006).

RS3594 was tested at concentrations corresponding to about 100- or 1000-fold of its IC_{50}, consistent with the activity of these nuclear-target compounds in cells. The choice of AMD3100 was based on literature data.

As depicted in Fig. 4, the dual MDMs ligand induced a significant accumulation of p53. Interestingly, AMD3100 also accumulated p53 protein (Fig. 4A and B), suggesting that a CXCR4 antagonism can trans-reactivate the p53 pathway. CXCR4 activation has repeatedly proven to reduce neuronal p53 content (Khan et al., 2005). The combined AMD3100 and RS3594 treatment demonstrated

an enhanced p53 protein accumulation compared to cells treated with either AMD3100 or RS3594 alone (Fig. 4A and B and Figure S2). As a second step, Real-Time PCR analysis was conducted to assess the transcriptional activity of p53. As depicted in Fig. 4C, RS3594 caused significant induction of the p53-target gene, MDM2. Remarkably, similar results were observed when treating cells with AMD3100. Moreover, RS3594 induced a significant enhancement in PUMA and p21 mRNA expression compared to control cells (Fig. 4D). The p53-upregulated modulator of apoptosis (PUMA) is a promoter of apoptosis that is induced in response to ER stress and directly attaches to the Bcl-2 and antagonizes this anti-apoptotic mediator (Najafi et al., 2019).

These findings prove that RS3594 and AMD3100 were able to reactivate p53. Then, in order to investigate a link between the p53/MDMs axis and CXCR4 in GBM, the assay was carried out in the presence of the CXCR4 antagonist AMD3100. When combined, the two compounds showed a significantly greater upregulation of MDM2 mRNA (Fig. 4C) with respect to the single-treated cells. It can be concluded that the CXCR4 receptor antagonism synergizes in reactivating the p53 pathway when combined with a disruptor of the MDMs-p53 complex.

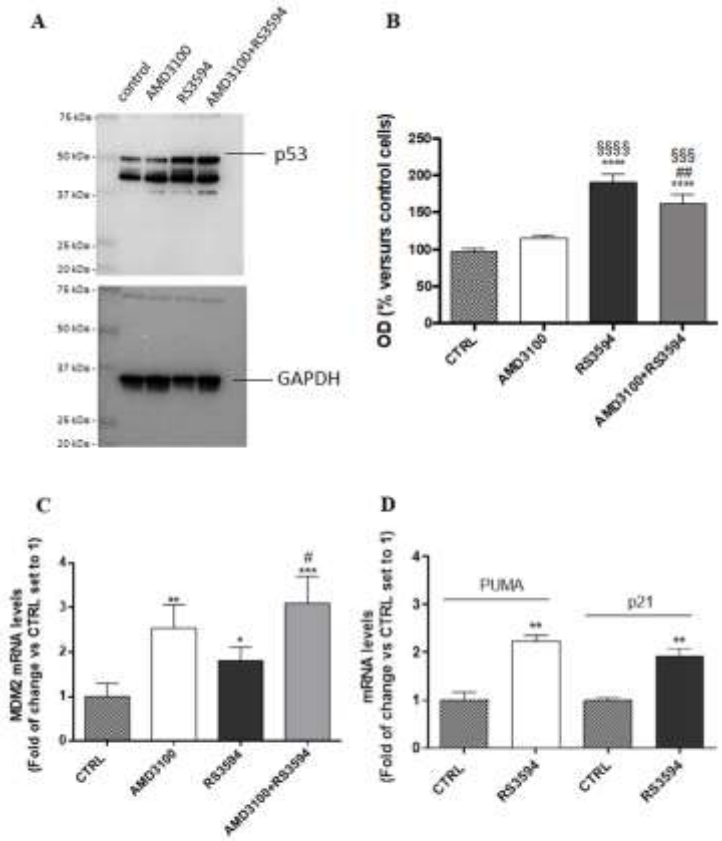

Fig. 4. Effects of RS3594 and AMD3100 on the p53 pathway's reactivation. (A, B) U87MG cells were treated with RS3594 (1 μM) and AMD3100 (10 μM), alone or in combination, for 24 h. Cell lysates were subjected to western blot analysis using a specific antibody for p53. GAPDH was used as the loading control. A representative image is shown in panel A. (B) Densitometric analysis was performed using ImageJ software. The data are shown as optical density (OD) versus control cells. (C, D) U87MG cells were treated with RS3594 (1 μM) and AMD3100 (10 μM), alone or in combination, for 8 h. Following treatments, total RNA was extracted and the expression levels of MDM2, p21, and PUMA were evaluated by quantitative Real-Time RT-PCR, as reported in the experimental section. The data are expressed as the fold change versus control level (mean values ± SD of three different experiments performed in duplicate). $^{*}p<0.05$, $^{**}p<0.01$ and $^{***}p<0.001$ versus the control. $^{\#}p<0.05$ and $^{\#\#\#}p<0.001$ versus cells treated with RS3594. $^{\$\$\$}p<0.001$ versus the cells treated with AMD3100.

3.5 Anti-proliferative effects of RS3594 in GBM cells. Following the demonstration of the p53 reactivation, the cell viability was assessed upon GBM cell treatment with RS3594, in the absence or presence of AMD3100. In particular, the compounds were tested for their anti-proliferative effects in the GBM cell lines (U87MG and U343MG cells) expressing a wild-type p53. Moreover, considering the proven efficacy of CXCR4 blockers in breast cancer, the breast cancer cells (MCF-7) were used as a comparison in selected experiments. Both cell lines have been demonstrated to express MDM2/4 (Wang et al., 2014) and CXCR4 receptors (Mercurio et al., 2016).

Compound RS3594 induced a significant inhibition of U87MG cell proliferation, following 72 h of incubation, with an IC_{50} of 1.37 µM (Fig. 5A). Similar results were obtained in MCF-7 cells (IC_{50} 1.9 µM, Fig. 5B). Moreover, RS3594 induced a significant inhibition of U343MG cell proliferation following 72 h of incubation, with a maximum effect comparable to that obtained in U87MG cells (Fig. 5C). In contrast, the anti-proliferative effects were significantly lower in p53-mutated cells (i.e., T98G cells, Fig. 5C) with respect to p53-wild type GBM cells. These data demonstrate that RS3594 acts through p53-dependent mechanisms, at least in the tested GBM cells.

In contrast, compound AMD3100 did not significantly affect cellular proliferation at 10 µM neither in U87MG (Fig. 5D) nor in MCF-7 (data not shown) cells. Nevertheless, when RS3594 (10 µM) was added to AMD3100-treated cells, a significant reduction in the percentage of proliferative cells was detected (Fig. 5D). The observed effects were significantly higher when compared to single-compound treated cells (Fig. 5C). These results demonstrate that AMD3100 sensitized glioma cells to the anti-proliferative action of RS3594.

To test the putative toxicity of the compounds on non-cancer cells, the microglia C20 cell line was employed for viability assays. As depicted in Fig. 5 (panel E), the highest concentrations of AMD3100 and RS3594 appreciably decreased the proliferation rate of microglia cells. The percentage of cell proliferation was ~~-~~higher in microglia C20 cell line than U87MG ~~treated~~ after treatment with RS3594 alone (74% vs 46%, P = 0,0092, respectively~~, respectively~~) and in combination with AMD3100 (88% vs 39%, P = 0,0026, respectively~~, respectively~~). ~~was higher in microglia C20 cell line than U87MG.~~

Furthermore, we investigated if the antiproliferative effects of the compounds could be associated with apoptosis. The number of living, early and late apoptosis cells were ~~analyzed~~analysed by Annexin assay. After treatment, RS3594 and the co-treatment were able to significantly enhance the percentage of cells in the early apoptosis (Figure S3), suggesting an apoptosis activation.

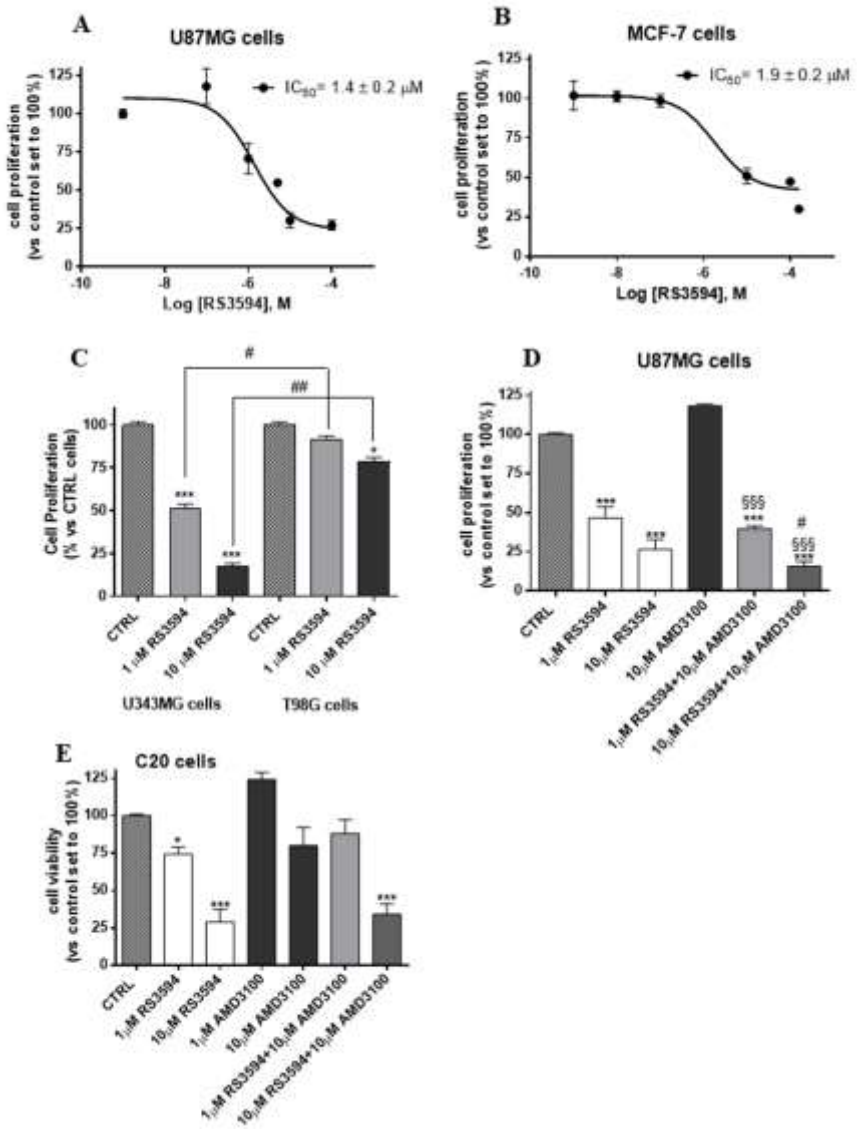

Fig. 5. Effect of RS3594 and AMD3100 on cell proliferation. U87MG (A) and MCF-7 (B) were treated with increasing concentrations (1 nM-100 μM) of RS3594. (C) U343MG and T98G were treated with RS3594 (1μM and 10μM). U87MG (D) and C20 cells (E) were treated with RS3594 (1μM and 10μM) and AMD3100 (1 μM and 10 μM), alone or in combination. Following 72 h, cell viability was evaluated by MTS assay as described in the experimental section. Data are reported as a percentage

with respect to control, set to 100% (mean ± SD of three different experiments conducted in triplicate). *p<0.05, ***p<0.001 vs the control. $^{\#}p$<0.05 versus cells treated with RS3594. $^{\$\$\$}p$<0.001 versus the cells treated with AMD3100.

3.6 RS3594 synergizes with AMD3100 in reducing GBM cells migration and invasiveness. Given the pivotal role of CXCR4 in controlling cell migration and invasiveness (Guo et al., 2014; Niu et al., 2015), and the interplay registered in breast cancer between MDMs and CXCR4, additional experiments were conducted to investigate the effects of AMD3100, alone or in combination with the MDM2/4 inhibitor RS3594 in GBM (U87MG cells).

First, a Matrigel assay was performed on control and treated cells by counting invading cells on the lower surface of the transwell membrane after fixing with p-formaldehyde and staining with crystal violet (Nuti et al., 2011). The results showed that the CXCR4 blocker (AMD3100) significantly reduced the percentages of invading cells compared to untreated samples (Fig. 6A and B). A significant reduction of U87MG cellular invasiveness was evident also in samples treated with RS3594 (Fig. 6A and B), tested at 1 μM and 10 μM, in a concentration-dependent manner. When cells were incubated simultaneously with AMD3100 and RS3594, additive/synergic effects were noticed (Fig. 6A and B). Because the reduction in cell viability at 24 h, in particular for AMD3100, was not significant following 24 h of incubation (data not shown), these results may be ascribed to an invasion phenomenon rather than a decrease in cell number.

To confirm these data, a wound-healing assay was performed. In particular, cells were scratched and then treated with RS3594, alone or in combination with AMD3100, for 24 h. As depicted in Fig. 7, AMD3100 significantly reduced the migration distance of U87MG cells with respect to control cells. Quantitative analysis of the gap area proved that the MDM2/4 inhibitor (RS3594, 1 μM) significantly decreased glioma migration (Fig. 7A and B). When GBM cells were challenged with AMD3100 and RS3594 simultaneously, the gap area increased (Fig. 7A and B) with respect to untreated and single-treated cells, thus reducing the glioma migration.

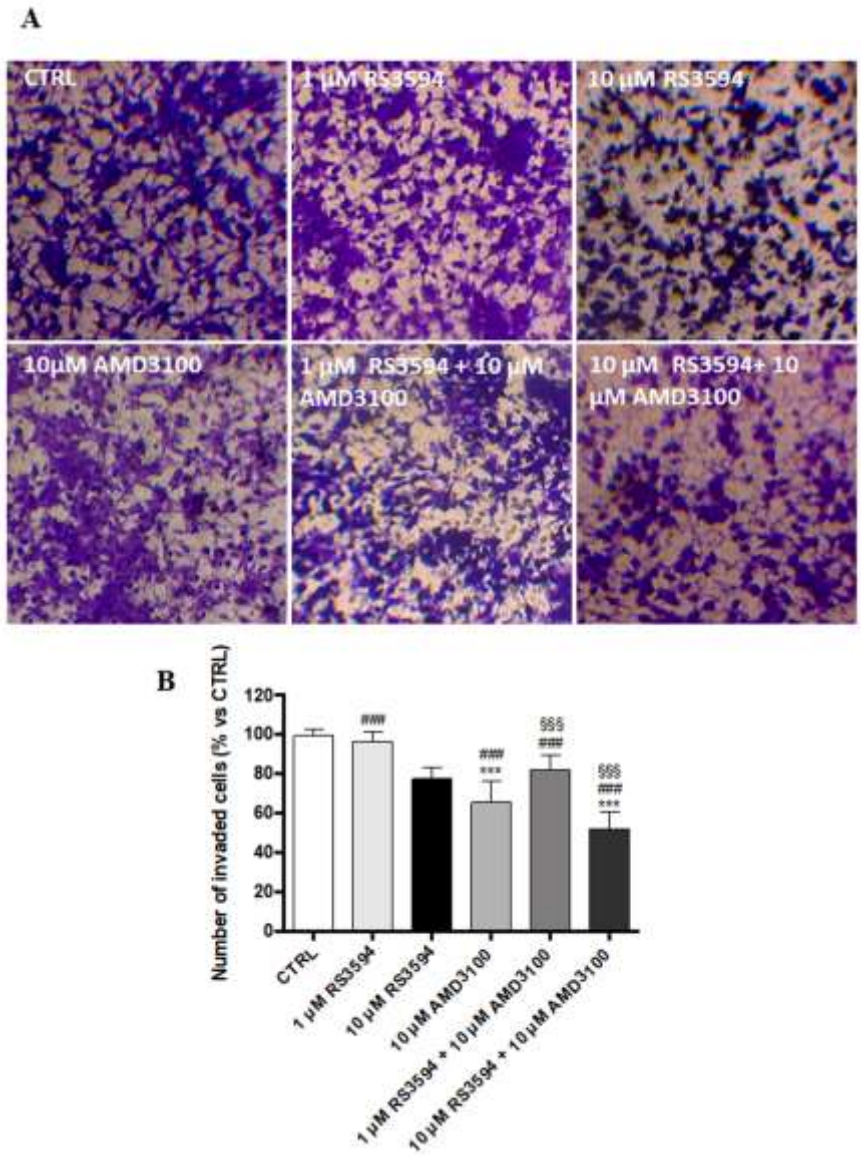

Fig. 6. Effect of RS3594 and AMD3100 on U87MG cell invasiveness. Cell invasion was analyzed through the Matrigel basement membrane transwell system, as described in the experimental section. (A) Representative images of U87MG incubated with RS3594 (10 µM and 1 µM) and AMD3100 (10 µM) alone or in combination for 24 h. (B) Cell invasiveness was measured by counting the number of cells that migrated into the lower face of the transwell membrane. $^{***}p<0.001$ versus control. $^{###}p<0.001$,

$^{\#\#}p<0.01$ versus cells treated with RS3594 (10 µM). $^{\S\S\S}p<0.001$ versus cells treated with AMD3100 (10 µM).

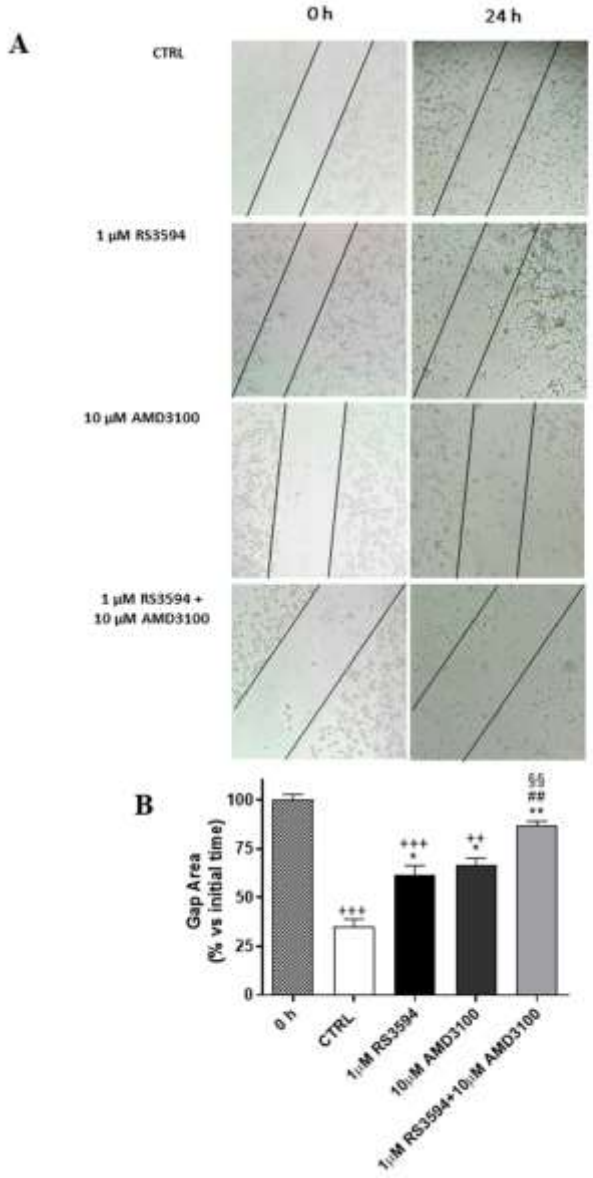

Fig. 7. Effect of RS3594 and AMD3100 on U87MG cell migration. The cells were treated with RS3594 (1 µM) and AMD3100 (10 µM), alone or in combination, and the healing of the scratch wounds was evaluated. A) Representative pictures of the scratch wounds at 0 h and 24 h. Dashed lines were shown in the images. B) The percentage of gap closure compared to the respective gap at t0. The data are presented as the means ± SD of at least two different experiments performed in triplicate. $^{++}p<0.01$ and $^{+++}p<0.001$ versus 0 h. $^{*}p<0.05$ and $^{**}p<0.01$ versus the control. $^{\#\#}p<0.01$ versus the cells treated with RS3594 (1 µM). $^{\S\S}p<0.01$ versus the cells treated with AMD3100 (10 µM).

3.7 RS3594 synergizes with AMD3100 enhancing the anti-proliferative and anti-clonogenic effects in GSCs. As mentioned above, GBM stem-like cells (GSCs) have been proven to possess a high tumorigenic capacity and a significant radio- and chemo-resistance, highlighting the need for a "stem cell-oriented therapy" to reduce ~~tumor~~tumour recurrence and improve GBM prognosis (Daniele et al., 2015a; Liu et al., 2006). In this sense, both CXCR4 and p53/MDMs axis (Daniele et al., 2015a; Yu et al., 2016) have been demonstrated to affect the proliferation of neurospheres (Miyazaki et al., 2017).

Therefore, further experiments were performed to assess the effects of RS3594 on neurospheres. Particularly, studies were carried out on the stem cell component of U87MG cells by culturing the cells in a defined serum-free medium that allows isolating cancer stem cells as "neurospheres" (Daniele et al., 2018, 2017b, 2015a, 2015b). These cells were demonstrated to present an enhancement in the mRNA expression of the stem cell marker (CD133) and a decrease of the glial marker GFAP (glial fibrillary acidic protein, Figure S4), confirming the validity of this established protocol (Daniele et al., 2018, 2017b, 2015a, 2015b, 2014b; Giacomelli et al., 2017). The use of these spheroids as a GSC model presents undoubtedly some limitations but can be a starting point to test the efficacy of new compounds in a cell subpopulation that is richer of cancer stem cells.

Fig. 8A shows representative images of neurospheres treated for seven days with RS3594, alone or in combination with AMD3100. Observing the results, RS3594 reduced significantly the number and the area (Fig. 8A and B and C) of neurospheres in culture. Of note, the first effect occurred in a concentration-dependent manner. In contrast, AMD3100 did not affect their area (Fig. 8A and C), but it slightly reduced their number when used at 10 µM (Fig. 8A and B). The area of neurospheres (Fig. 8A and C) was significantly decreased when AMD3100 was combined with RS3594, although with a percentage of reduction comparable to those observed with RS3594 alone. Interestingly, AMD3100 was proven to induce cellular sprouting of cultured neurospheres (Fig. 8A and D), suggesting that blocking CXCR4 can induce their differentiation.

Next, the ability of RS3594 on the formation of neurospheres was verified by clonogenic assay. To this purpose, neurospheres were dissected and a clonogenic assay was performed after 7 days of treatment with subtoxic concentrations of AMD3100 or RS3594 for this assay (Fig. 9A and B and Figure

S5). In particular, it was pivotal to use non-toxic concentrations of the compounds in this assay. Otherwise, the reduction in the clonogenic potential could be ascribed to a toxic effect rather than an inhibition of the cell clonogenic ability.

RS3594 significantly reduced the total sphere number (Fig. 9A and B) in a concentration-dependent manner. Similar results were obtained with AMD3100 (Fig. 9A and B). When the lowest concentration of RS3594 was combined with the lowest concentration of AMD3100, the anti-clonogenic effect was enhanced compared to single-treated cells (Fig. 9A and B).

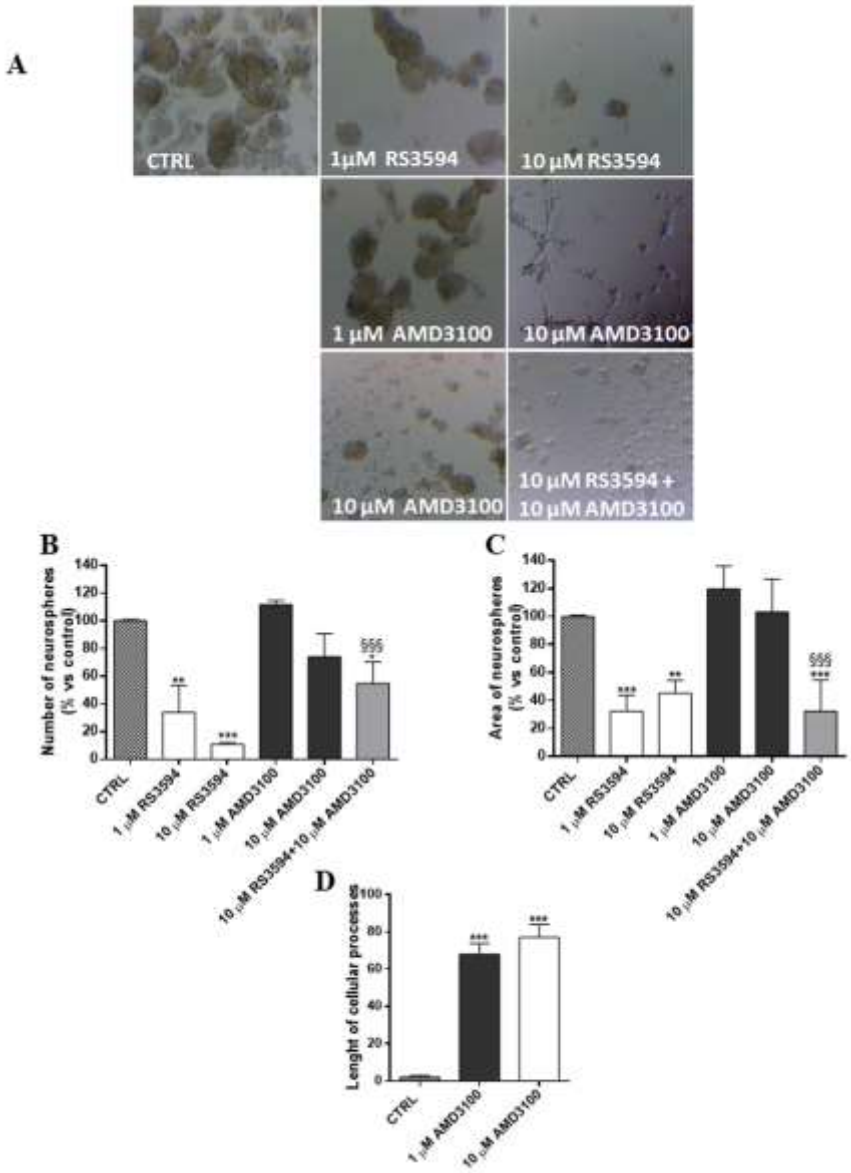

Fig. 8. Effects of RS3594 and AMD3100 on sphere-derived cell morphology. Neurospheres were treated for 7 days with RS3594 (1 µM and 100 µM) and AMD3100 (1 µM and 10 µM) in complete NSC medium. (A) Representative pictures of the neurospheres after 7 days of incubation were shown. The number (B), area (C), and length of cellular processes (D) of the newly formed spheres were scored after 7 days of treatments. The data represent the mean ± SD of three pictures from two different

experiments. $^{*}p<0.05$, $^{**}p<0.01$, $^{***}p<0.001$versus the control. $^{§§§}p<0.001$ versus the cells treated with AMD3100 (10 µM).

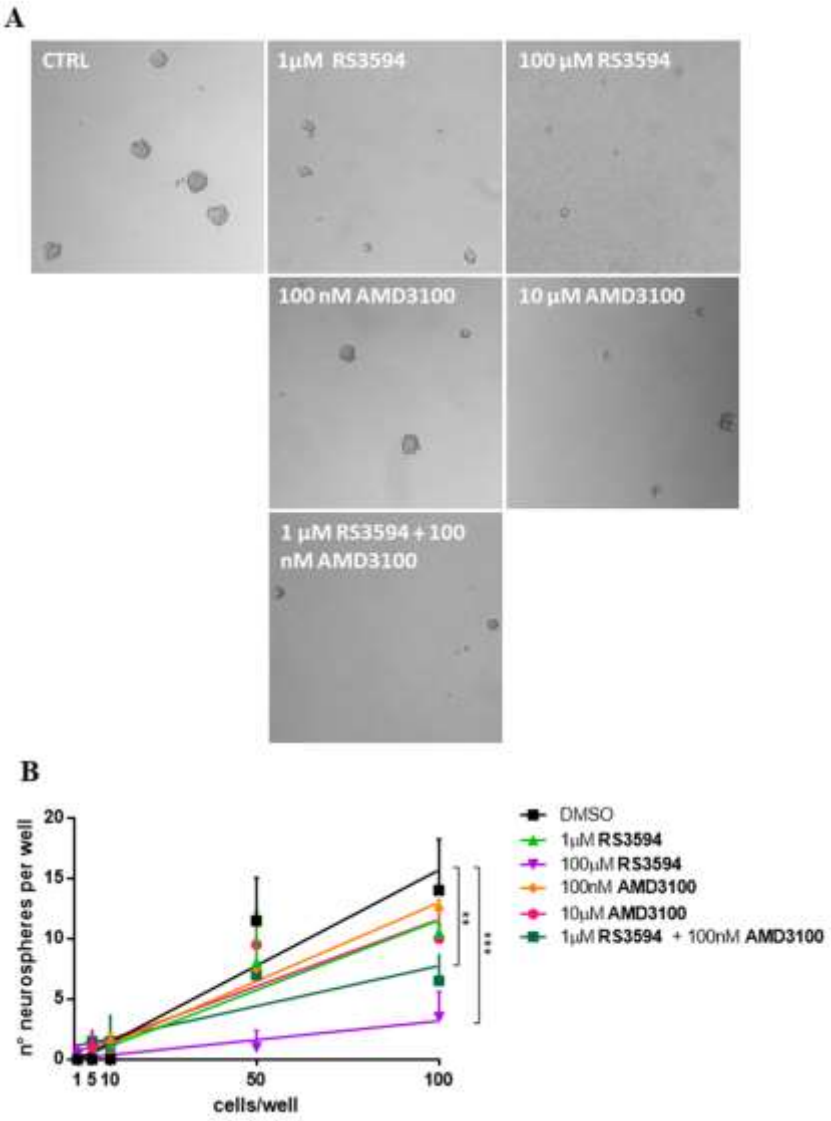

Fig. 9. Effects of RS3594 and AMD3100 on the clonogenic potential of GBM cells. (A) Representative microscopic images of neurospheres (100 cells/well) after 7 days of treatment with RS3594 (1 μM and 100 μM) and AMD3100 (100 nM and 10 μM), alone or in combination. (B) Quantitative results of the clonogenic assay. Data are presented as the mean ± SD of two different experiments. $^{**}p<0.01$, $^{***}p<0.001$ versus the control, as indicated in panel B.

4. Discussion (MAX 1500 words)

In the present study, a rationally designed MDM2/4 inhibitor was combined with the CXCR4 antagonist, AMD3100, in human GBM cells, and tested in GBM stem-like cells (neurospheres), which are crucial for tumor recurrence and chemotherapy resistance. The dual MDM2/4 inhibitor RS3594 and the CXCR4 antagonist AMD3100 reduced GBM cell invasiveness and migration in single-agent treatment and mainly in combination. Of note, two compounds present synergic effects on cancer stem component: RS3594 efficiently blocks the growth of neurospheres and inhibits their formation (Fig. 8B and C), while AMD3100 induces the differentiation of neurospheres (Fig. 8D), and acts synergistically with RS3594 in blocking their proliferation and clonogenic ability (Fig. 9A and B). These results confirm that blocking CXCR4/MDM2/4 represents a valuable strategy to reduce GBM proliferation and invasiveness, acting on the stem cell component too**.**

GBM is one of the most aggressive and deadly forms of human cancer. Growing evidence has highlighted that the use of combined therapies can enhance the effectiveness of reducing the tumor mass and prevent tumor recurrence. Moreover, a stem cell-oriented treatment would be the most effective strategy to contrast GBM aggressiveness and invasive nature, and in turn to reduce recurrence and improve GBM prognosis (Liu et al., 2006). At a molecular level, GBM is characterized by an overexpression of murine double minute proteins 2 and 4 (MDM2 and MDM4), which inactivate p53 by targeting it through ubiquitin degradation or by inhibiting its functional binding to DNA, leading to loss of tumor suppressor functions including growth arrest, apoptosis, DNA repair, and senescence (Zhang et al., 2018). Anomalies in the p53-MDMs pathway are associated with GBM progression and are related to a less apoptotic, more invasive, and more stem-like phenotype (Zhang et al., 2018). A great variety of MDM2 inhibitors have been developed to counteract the hyperactivation of MDMs, in order to treat GBM and other tumors. In particular, recent data suggest that a complete p53 reactivation and a permanent, effective clinical response can only be accomplished by targeting both MDM proteins simultaneously (Burgess et al., 2016; Sestito et al., 2018). Indeed, the two homologous proteins can function independently on p53, but they can increase their effectiveness, forming an MDM2/4 heterodimer.

An aberrant tumoral p53-MDMs axis has been frequently related to the CXCR4 signaling. In particular, CXCR4 activation stimulates MDM2 expression and inhibits p53, promoting cancer cell growth (Arcarolli et al., 2009). Of note, CXCR4 is overexpressed in both GBM and GSCs, and its

expression correlates with GBM malignancy, grade, and invasive nature as well as poor prognosis AGGIUNGERE REF https://doi.org/10.1016/j.lfs.2020.117534 (Bian et al., 2007; Presti et al., 2018). Overall, these data suggest CXCR4 and MDM2/4 may cooperate in promoting tumor progression and invasion in GBM too, as well as in breast and pancreatic cancer, and the blocking of CXCR4 and MDMs proteins could lead to a complete p53 reactivation in GBM cells and the GSC counterpart.

On this basis, a potent dual MDM2/4 inhibitor has been used in the present paper as a probe to shed light on the interplay between the MDMs axis and the CXCR4 receptor in human GBM. The novel dual MDM2/4 inhibitor RS3594 has been discovered thanks to the rational optimization of its precursor 3, identified through a previously published Receptor-Based Virtual Screening. NMR and modeling studies were performed to reveal its modality of binding to the canonical pocket of MDMs. The ability of the to dissociate p53 from MDM2 and MDM4 was analyzed with an immunoenzymatic assay using cell lysates expressing high levels of the p53-MDM2 and p53-MDM4 complexes (Daniele et al., 2016, 2014a).

The dual MDMs ligand induced a significant accumulation of p53 (Fig. 4A and B) and a significant induction of the p53-target genes (Fig. 4C). The CXCR4 antagonist also accumulated p53 protein (Fig. 4A and B) and enhanced MDM2 mRNA (Fig. 4C), suggesting that a CXCR4 antagonism can trans-reactivate the p53 pathway. Consistent with our data, CXCR4 activation has repeatedly proven to reduce neuronal p53 content (Khan et al., 2005) and, conversely, CXCR4-mediated cancer cell migration and invasion is attenuated by p53 activation (Werfel et al., 2018).

When combined, the two compounds showed a significantly greater upregulation of p53 protein accumulation and MDM2 mRNA with respect to the single-treated cells (Fig. 4A-C). It can be concluded that the CXCR4 receptor antagonism synergizes in reactivating the p53 pathway when combined with a disruptor of MDMs-p53 complex. These data are in accordance with those obtained in breast cancer cells, in which CXCR4 antagonist has been shown to sensitize breast cancer cells to ionizing radiation by promoting p53 accumulation and reactivating the p53/Bax pro-apoptotic pathways (Zhou et al., 2018).

Then, the compounds were tested for their anti-proliferative effects in the GBM cell lines (U87MG and U343MG cells) expressing a wild-type p53. RS3594 induced a significant inhibition of U87MG cell proliferation with an IC_{50} of 1.37 μM in U87MG cells (Fig. 5A and C). In contrast, the anti-proliferative effects were significantly lower in p53-mutated cells (i.e. T98G cells) with respect to p53-wild type GBM cells, confirming that the compound acts through p53-dependent mechanisms, at least in the tested GBM cells (Fig. 5C). As demonstrated for less potent derivatives of RS3594 (Giustiniano et al., 2017), we may hypothesize an apoptotic mechanism at the basis of the anti-proliferative effect. Moreover, this effect may be consistent with the induction of PUMA mRNA induced by RS3594. In contrast, compound AMD3100 did not significantly affect GBM cellular proliferation. Consistent with our data, the CXCR4 blocker has proven to reduce the viability of different tumor cells only at very high

concentrations (Berning et al., 2018; Jung et al., 2016). However, since compound AMD3100 has been demonstrated to improve the sensitivity of radiotherapy in several types of cancer (Ali et al., 2013; Domanska et al., 2014), we decided to test this compound in combination with RS3594 in U87MG cells. When RS3594 was added to AMD3100-treated cells, the observed antiproliferative effects were significantly higher when compared to single-compound treated cells (Fig. 5D). These results demonstrate that AMD3100 sensitized glioma cells to the anti-proliferative action of RS3594 and are consistent with literature data demonstrating that CXCR4 inhibition with AMD3100 sensitizes cancer cells to chemotherapy (Ali et al., 2013; Domanska et al., 2014, 2012). RS3594 caused a significant reduction of U87MG cellular invasiveness, in a concentration-dependent manner, confirming that p53 reactivation can control the processes of cancer cell invasion (Bieging et al., 2014). The CXCR4 blocker significantly reduced the percentages of invading cells compared to untreated samples, consistent with the established role of CXCR4 in cancer cell migration and invasiveness (Guo et al., 2014; Niu et al., 2015), including glioma (Ehtesham et al., 2006). When cells were incubated simultaneously with AMD3100 and RS3594, additive/synergic effects were noticed, suggesting that the dual inhibitor RS3594 efficiently suppresses U87MG cell migration/invasiveness and that additive/synergic effects can occur when combined with the CXCR4 blocker AMD3100 (Fig. 6A and B and Fig, 7A and B).

Finally, the combined action of RS3594 and AMD3100 was tested in spheroids used as a model of GBM stem-like cells (GSCs), which have been emerging as a target to reduce tumor recurrence and improve GBM prognosis (Daniele et al., 2015a; Liu et al., 2006).

RS3594 reduced significantly the number and the area of neurospheres in culture (Fig. 8B and C), confirming that the dissociation of p53 from MDM2/4 is a valuable strategy to reduce the proliferation of neurospheres (Daniele et al., 2015a; Yu et al., 2016). AMD3100 slightly reduced the spheroids number and induced cellular sprouting of cultured neurospheres (Fig. 8B-D), suggesting that blocking CXCR4 can induce their differentiation. Consistent with our findings, the CXCR4 antagonist has been demonstrated to control CSC proliferation (Miyazaki et al., 2017), and the novel CXCR4 antagonist PRX177561 has been recently demonstrated to accelerate CSC differentiation in glioblastoma preclinical models (Gravina et al., 2017).

A clonogenic assay confirmed that RS3594 and AMD3100 were able to reduce spheroid formation. When combined together, the anti-clonogenic effect was enhanced compared to single-treated cells, demonstrating that combining MDM2/4 dissociation from p53 with a block of CXCR4 can greatly inhibit neurosphere formation (Fig. 9A and B).

Globally, our data showed that the inhibition of the two pathways synergistically reduces the invasiveness and the migration of GBM cells and that the CXCR4 antagonist AMD3100 is able to sensitize GBM cells to the anti-proliferative activity of the dual MDMs inhibitor RS3594. Of most importance, the experiments herein reported, demonstrated that similar to what happens in breast cancer,

the two pathways greatly affect the stem cell component of the GBM. These results confirm that the CXCR4/MDM2/4 block can represent a valuable strategy to reduce GBM proliferation and invasiveness, acting, most importantly, on the stem cell component. Of note, the efficacy of the proposed therapeutic strategy is limited to GBM ~~tumors~~tumours expressing wild-type p53. Specific compounds are needed in the case of a mutated p53 since conventional reactivators would not be effective.

Supplementary Materials:– Chemical synthesis of compounds. Scheme 1, synthesis of compounds 3 and 4. Scheme 2, synthesis of compounds 5 and 9. Scheme 3, synthesis of compounds 6 and 12. Scheme 4, synthesis of compounds 7, 10 and 11. Scheme 5, synthesis of compounds 8 and 13 (RS3594). Evaluation of blood-brain barrier permeability. Table S1 and Figure S1, ability of RS3594 to cross the blood-brain barrier. Figure S2, effects of RS3594 and AMD3100 on the p53 protein accumulation. Figure S3, effects of RS3594 and AMD3100 on apoptosis. ~~effects of RS3594 on the p53 target genes.~~ Figure S4, differentiation and stemness markers in neurospheres derived from GBM cells. Figure S5, effects of RS3594 and AMD3100 on the clonogenic potential of GBM cells.

AUTHOR CONTRIBUTIONS: Conceptualization, S.D., and V.L.P.; methodology and experimental procedures, S.D., D.P, R.P., C.C., V.M.A, M.N. and L.C; formal analysis, M.F. and C.L.; investigation, D.P, R.P., C.C., V.M.A, L.C., S.G., P.R., M.P., M.F. and M.P.; data curation, S.D. and V.L.P; writing—original draft preparation, S.D. and V.L.P; writing—review and editing S.T., L.M. and C.M; supervision, G.L.R., R.S., E,N. and C.M.; project administration, E.N. and R.S; funding acquisition, R.S., C.M., L.M., and E.N. All authors have agreed to the final version of the manuscript.

DECLARATIONS OF INTEREST: none

FUNDING SOURCES: This research was funded by Italian PRIN 2015 (FCHJ8E to R.S. and L.M.), Regione Campania-POR Campania FESR 2014/2020 (Project N. B61G18000470007), Sapienza Università di Roma (RP11715C7D1CF0D1 and RM11916B5598E3C4 to G.L.R. and RG11816428A9B4D5 to R.S.), Italian Ministry of Education, University and Research- Dipartimenti di Eccellenza - L.232/2016 (to M.P., M.N., G.L.R., R.S) and Istituto Pasteur Italia – Fondazione Cenci Bolognetti (Call 2019 to G.L.R.).

REFERENCES

Ali, M.M., Kumar, S., Shankar, A., Varma, N.R.S., Iskander, A.S.M., Janic, B., Chwang, W.B., Jain, R., Babajeni-Feremi, A., Borin, T.F., Bagher-Ebadian, H., Brown, S.L., Ewing, J.R., Arbab, A.S., 2013. Effects of Tyrosine Kinase Inhibitors and CXCR4 Antagonist on Tumor Growth and Angiogenesis in Rat Glioma Model: MRI and Protein Analysis Study. Transl Oncol 6, 660–669.

Arcarolli, J., Pike, L., Messersmith, W., Weekes, C., 2009. Abstract #1102: CXCR4 activation stimulates MDM2 in a mTOR-dependent manner to promote pancreas tumor growth. Cancer Res 69, 1102–1102.

Berning, P., Schaefer, C., Clemens, D., Korsching, E., Dirksen, U., Potratz, J., 2018. The CXCR4 antagonist plerixafor (AMD3100) promotes proliferation of Ewing sarcoma cell lines in vitro and activates receptor tyrosine kinase signaling. Cell Communication and Signaling 16, 21. https://doi.org/10.1186/s12964-018-0233-2

Bian, X., Yang, S., Chen, J., Ping, Y., Zhou, X., Wang, Q., Jiang, X., Gong, W., Xiao, H., Du, L., Chen, Z., Zhao, W., Shi, J., Wang, J.M., 2007. Preferential expression of chemokine receptor CXCR4 by highly malignant human gliomas and its association with poor patient survival. Neurosurgery 61, 570–578; discussion 578-579. https://doi.org/10.1227/01.NEU.0000290905.53685.A2

Bieging, K.T., Mello, S.S., Attardi, L.D., 2014. Unravelling mechanisms of p53-mediated tumour suppression. Nature Reviews Cancer 14, 359–370. https://doi.org/10.1038/nrc3711

Burgess, A., Chia, K.M., Haupt, S., Thomas, D., Haupt, Y., Lim, E., 2016. Clinical Overview of MDM2/X-Targeted Therapies. Front. Oncol. 6. https://doi.org/10.3389/fonc.2016.00007

Cancer Genome Atlas Research Network, 2008. Comprehensive genomic characterization defines human glioblastoma genes and core pathways. Nature 455, 1061–1068. https://doi.org/10.1038/nature07385

Chang, Y.S., Graves, B., Guerlavais, V., Tovar, C., Packman, K., To, K.-H., Olson, K.A., Kesavan, K., Gangurde, P., Mukherjee, A., Baker, T., Darlak, K., Elkin, C., Filipovic, Z., Qureshi, F.Z., Cai, H., Berry, P., Feyfant, E., Shi, X.E., Horstick, J., Annis, D.A., Manning, A.M., Fotouhi, N., Nash, H., Vassilev, L.T., Sawyer, T.K., 2013. Stapled α-helical peptide drug development: a potent dual inhibitor of MDM2 and MDMX for p53-dependent cancer therapy. Proc. Natl. Acad. Sci. U.S.A. 110, E3445-3454. https://doi.org/10.1073/pnas.1303002110

Daniele, S., Costa, B., Da Pozzo, E., Sestito, S., Nesi, G., Campiglia, P., Marinelli, L., Novellino, E., Rapposelli, S., Martini, C., 2015a. Combined inhibition of AKT/mTOR and MDM2 enhances Glioblastoma Multiforme cell apoptosis and differentiation of cancer stem cells. Sci Rep 5, 9956. https://doi.org/10.1038/srep09956

Daniele, S., Giacomelli, C., Zappelli, E., Granchi, C., Trincavelli, M.L., Minutolo, F., Martini, C., 2015b. Lactate dehydrogenase-A inhibition induces human glioblastoma multiforme stem cell differentiation and death. Sci Rep 5, 15556. https://doi.org/10.1038/srep15556

Daniele, S., La Pietra, V., Barresi, E., Di Maro, S., Da Pozzo, E., Robello, M., La Motta, C., Cosconati, S., Taliani, S., Marinelli, L., Novellino, E., Martini, C., Da Settimo, F., 2016. Lead Optimization of 2-Phenylindolylglyoxylyldipeptide Murine Double Minute (MDM)2/Translocator Protein (TSPO) Dual Inhibitors for the Treatment of Gliomas. J. Med. Chem. 59, 4526–4538. https://doi.org/10.1021/acs.jmedchem.5b01767

Daniele, S., Natali, L., Giacomelli, C., Campiglia, P., Novellino, E., Martini, C., Trincavelli, M.L., 2017a. Osteogenesis Is Improved by Low Tumor Necrosis Factor Alpha

Concentration through the Modulation of Gs-Coupled Receptor Signals. Mol. Cell. Biol. 37. https://doi.org/10.1128/MCB.00442-16

Daniele, S., Pietrobono, D., Costa, B., Giustiniano, M., La Pietra, V., Giacomelli, C., La Regina, G., Silvestri, R., Taliani, S., Trincavelli, M.L., Da Settimo, F., Novellino, E., Martini, C., Marinelli, L., 2018. Bax Activation Blocks Self-Renewal and Induces Apoptosis of Human Glioblastoma Stem Cells. ACS Chem Neurosci 9, 85–99. https://doi.org/10.1021/acschemneuro.7b00023

Daniele, S., Sestito, S., Pietrobono, D., Giacomelli, C., Chiellini, G., Di Maio, D., Marinelli, L., Novellino, E., Martini, C., Rapposelli, S., 2017b. Dual Inhibition of PDK1 and Aurora Kinase A: An Effective Strategy to Induce Differentiation and Apoptosis of Human Glioblastoma Multiforme Stem Cells. ACS Chem Neurosci 8, 100–114. https://doi.org/10.1021/acschemneuro.6b00251

Daniele, S., Taliani, S., Da Pozzo, E., Giacomelli, C., Costa, B., Trincavelli, M.L., Rossi, L., La Pietra, V., Barresi, E., Carotenuto, A., Limatola, A., Lamberti, A., Marinelli, L., Novellino, E., Da Settimo, F., Martini, C., 2014a. Apoptosis therapy in cancer: the first single-molecule co-activating p53 and the translocator protein in glioblastoma. Sci Rep 4, 4749. https://doi.org/10.1038/srep04749

Daniele, S., Zappelli, E., Natali, L., Martini, C., Trincavelli, M.L., 2014b. Modulation of A1 and A2B adenosine receptor activity: a new strategy to sensitise glioblastoma stem cells to chemotherapy. Cell Death Dis 5, e1539. https://doi.org/10.1038/cddis.2014.487

Domanska, U.M., Boer, J.C., Timmer-Bosscha, H., Van, M.V., Hoving, H.D., Kliphuis, N.M., Rosati, S., Van, H. der P., De, I.J., De, E.V., Walenkamp, A.M., 2014. CXCR4 inhibition enhances radiosensitivity, while inducing cancer cell mobilization in a prostate cancer mouse model. Clin Exp Metastasis 31, 829–839. https://doi.org/10.1007/s10585-014-9673-2

Domanska, U.M., Timmer-Bosscha, H., Nagengast, W.B., Oude Munnink, T.H., Kruizinga, R.C., Ananias, H.J.K., Kliphuis, N.M., Huls, G., De Vries, E.G.E., de Jong, I.J., Walenkamp, A.M.E., 2012. CXCR4 Inhibition with AMD3100 Sensitizes Prostate Cancer to Docetaxel Chemotherapy. Neoplasia 14, 709–718. https://doi.org/10.1593/neo.12324

Ehtesham, M., Winston, J.A., Kabos, P., Thompson, R.C., 2006. CXCR4 expression mediates glioma cell invasiveness. Oncogene 25, 2801–2806. https://doi.org/10.1038/sj.onc.1209302

Friesner, R.A., Banks, J.L., Murphy, R.B., Halgren, T.A., Klicic, J.J., Mainz, D.T., Repasky, M.P., Knoll, E.H., Shelley, M., Perry, J.K., Shaw, D.E., Francis, P., Shenkin, P.S., 2004. Glide: a new approach for rapid, accurate docking and scoring. 1. Method and assessment of docking accuracy. J. Med. Chem. 47, 1739–1749. https://doi.org/10.1021/jm0306430

Friesner, R.A., Murphy, R.B., Repasky, M.P., Frye, L.L., Greenwood, J.R., Halgren, T.A., Sanschagrin, P.C., Mainz, D.T., 2006. Extra precision glide: docking and scoring incorporating a model of hydrophobic enclosure for protein-ligand complexes. J. Med. Chem. 49, 6177–6196. https://doi.org/10.1021/jm051256o

Gabelloni, P., Da Pozzo, E., Bendinelli, S., Costa, B., Nuti, E., Casalini, F., Orlandini, E., Da Settimo, F., Rossello, A., Martini, C., 2010. Inhibition of metalloproteinases derived from tumours: new insights in the treatment of human glioblastoma. Neuroscience 168, 514–522. https://doi.org/10.1016/j.neuroscience.2010.03.064

Gao, C., Xiao, G., Piersigilli, A., Gou, J., Ogunwobi, O., Bargonetti, J., 2019. Context-dependent roles of MDMX (MDM4) and MDM2 in breast cancer proliferation and circulating tumor cells. Breast Cancer Res 21. https://doi.org/10.1186/s13058-018-1094-8

Giacomelli, C., Daniele, S., Natali, L., Iofrida, C., Flamini, G., Braca, A., Trincavelli, M.L., Martini, C., 2017. Carnosol controls the human glioblastoma stemness features through the epithelial-mesenchymal transition modulation and the induction of cancer stem cell apoptosis. Sci Rep 7, 15174. https://doi.org/10.1038/s41598-017-15360-2

Giustiniano, M., Daniele, S., Pelliccia, S., La Pietra, V., Pietrobono, D., Brancaccio, D., Cosconati, S., Messere, A., Giuntini, S., Cerofolini, L., Fragai, M., Luchinat, C., Taliani, S., La Regina, G., Da Settimo, F., Silvestri, R., Martini, C., Novellino, E., Marinelli, L., 2017. Computer-Aided Identification and Lead Optimization of Dual Murine Double Minute 2 and 4 Binders: Structure-Activity Relationship Studies and Pharmacological Activity. J. Med. Chem. 60, 8115–8130. https://doi.org/10.1021/acs.jmedchem.7b00912

Gravina, G.L., Mancini, A., Colapietro, A., Vitale, F., Vetuschi, A., Pompili, S., Rossi, G., Marampon, F., Richardson, P.J., Patient, L., Patient, L., Burbidge, S., Festuccia, C., 2017. The novel CXCR4 antagonist, PRX177561, reduces tumor cell proliferation and accelerates cancer stem cell differentiation in glioblastoma preclinical models. Tumour Biol. 39, 1010428317695528. https://doi.org/10.1177/1010428317695528

Greenwood, J.R., Calkins, D., Sullivan, A.P., Shelley, J.C., 2010. Towards the comprehensive, rapid, and accurate prediction of the favorable tautomeric states of drug-like molecules in aqueous solution. J. Comput. Aided Mol. Des. 24, 591–604. https://doi.org/10.1007/s10822-010-9349-1

Guo, S., Xiao, D., Liu, H., Zheng, X., Liu, L., Liu, S., 2014. Interfering with CXCR4 expression inhibits proliferation, adhesion and migration of breast cancer MDA-MB-231 cells. Oncol Lett 8, 1557–1562. https://doi.org/10.3892/ol.2014.2323

Halgren, T.A., Murphy, R.B., Friesner, R.A., Beard, H.S., Frye, L.L., Pollard, W.T., Banks, J.L., 2004. Glide: a new approach for rapid, accurate docking and scoring. 2. Enrichment factors in database screening. J. Med. Chem. 47, 1750–1759. https://doi.org/10.1021/jm030644s

Hira, V.V.V., Verbovšek, U., Breznik, B., Srdič, M., Novinec, M., Kakar, H., Wormer, J., der Swaan, B.V., Lenarčič, B., Juliano, L., Mehta, S., Van Noorden, C.J.F., Lah, T.T., 2017. Cathepsin K cleavage of SDF-1α inhibits its chemotactic activity towards glioblastoma stem-like cells. Biochimica et Biophysica Acta (BBA) - Molecular Cell Research 1864, 594–603. https://doi.org/10.1016/j.bbamcr.2016.12.021

Hugon, B., Pfeiffer, B., Renard, P., Prudhomme, M., 2003. Synthesis of isogranulatimide analogues possessing a pyrrole moiety instead of an imidazole heterocycle. Tetrahedron Letters 44, 3927–3930. https://doi.org/10.1016/S0040-4039(03)00837-2

Jakalian, A., Jack, D.B., Bayly, C.I., 2002. Fast, efficient generation of high-quality atomic charges. AM1-BCC model: II. Parameterization and validation. J Comput Chem 23, 1623–1641. https://doi.org/10.1002/jcc.10128

Jorgensen, W.L., Chandrasekhar, J., Madura, J.D., Impey, R.W., Klein, M.L., 1983. Comparison of simple potential functions for simulating liquid water. J. Chem. Phys. 79, 926–935. https://doi.org/10.1063/1.445869

Jung, Y.H., Lee, D.Y., Cha, W., Kim, B.H., Sung, M.-W., Kim, K.H., Ahn, S.-H., 2016. Antitumor effect of CXCR4 antagonist AMD3100 on the tumorigenic cell line of BHP10-3 papillary thyroid cancer cells. Head Neck 38, 1479–1486. https://doi.org/10.1002/hed.24461

Khan, M.Z., Shimizu, S., Patel, J.P., Nelson, A., Le, M.-T., Mullen-Przeworski, A., Brandimarti, R., Fatatis, A., Meucci, O., 2005. Regulation of neuronal P53 activity by CXCR4. Mol Cell Neurosci 30, 58–66. https://doi.org/10.1016/j.mcn.2005.05.007

La Regina, G., Bai, R., Coluccia, A., Famiglini, V., Pelliccia, S., Passacantilli, S., Mazzoccoli, C., Ruggieri, V., Verrico, A., Miele, A., Monti, L., Nalli, M., Alfonsi, R., Di

Marcotullio, L., Gulino, A., Ricci, B., Soriani, A., Santoni, A., Caraglia, M., Porto, S., Da Pozzo, E., Martini, C., Brancale, A., Marinelli, L., Novellino, E., Vultaggio, S., Varasi, M., Mercurio, C., Bigogno, C., Dondio, G., Hamel, E., Lavia, P., Silvestri, R., 2015. New Indole Tubulin Assembly Inhibitors Cause Stable Arrest of Mitotic Progression, Enhanced Stimulation of Natural Killer Cell Cytotoxic Activity, and Repression of Hedgehog-Dependent Cancer. J. Med. Chem. 58, 5789–5807. https://doi.org/10.1021/acs.jmedchem.5b00310

La Regina, G., Bai, R., Rensen, W., Coluccia, A., Piscitelli, F., Gatti, V., Bolognesi, A., Lavecchia, A., Granata, I., Porta, A., Maresca, B., Soriani, A., Iannitto, M.L., Mariani, M., Santoni, A., Brancale, A., Ferlini, C., Dondio, G., Varasi, M., Mercurio, C., Hamel, E., Lavia, P., Novellino, E., Silvestri, R., 2011. Design and synthesis of 2-heterocyclyl-3-arylthio-1H-indoles as potent tubulin polymerization and cell growth inhibitors with improved metabolic stability. J. Med. Chem. 54, 8394–8406. https://doi.org/10.1021/jm2012886

La Regina, G., Bai, R., Rensen, W.M., Di Cesare, E., Coluccia, A., Piscitelli, F., Famiglini, V., Reggio, A., Nalli, M., Pelliccia, S., Da Pozzo, E., Costa, B., Granata, I., Porta, A., Maresca, B., Soriani, A., Iannitto, M.L., Santoni, A., Li, J., Miranda Cona, M., Chen, F., Ni, Y., Brancale, A., Dondio, G., Vultaggio, S., Varasi, M., Mercurio, C., Martini, C., Hamel, E., Lavia, P., Novellino, E., Silvestri, R., 2013. Toward highly potent cancer agents by modulating the C-2 group of the arylthioindole class of tubulin polymerization inhibitors. J. Med. Chem. 56, 123–149. https://doi.org/10.1021/jm3013097

Liu, G., Yuan, X., Zeng, Z., Tunici, P., Ng, H., Abdulkadir, I.R., Lu, L., Irvin, D., Black, K.L., Yu, J.S., 2006. Analysis of gene expression and chemoresistance of CD133+ cancer stem cells in glioblastoma. Mol. Cancer 5, 67. https://doi.org/10.1186/1476-4598-5-67

Liu, H., Wang, L., Lv, M., Pei, R., Li, P., Pei, Z., Wang, Y., Su, W., Xie, X.-Q., 2014. AlzPlatform: An Alzheimer's Disease Domain-Specific Chemogenomics Knowledgebase for Polypharmacology and Target Identification Research. J Chem Inf Model 54, 1050–1060. https://doi.org/10.1021/ci500004h

Maier, J.A., Martinez, C., Kasavajhala, K., Wickstrom, L., Hauser, K.E., Simmerling, C., 2015. ff14SB: Improving the Accuracy of Protein Side Chain and Backbone Parameters from ff99SB. J Chem Theory Comput 11, 3696–3713. https://doi.org/10.1021/acs.jctc.5b00255

Mercurio, L., Ajmone-Cat, M.A., Cecchetti, S., Ricci, A., Bozzuto, G., Molinari, A., Manni, I., Pollo, B., Scala, S., Carpinelli, G., Minghetti, L., 2016. Targeting CXCR4 by a selective peptide antagonist modulates tumor microenvironment and microglia reactivity in a human glioblastoma model. J. Exp. Clin. Cancer Res. 35, 55. https://doi.org/10.1186/s13046-016-0326-y

Merlino, F., Daniele, S., La Pietra, V., Di Maro, S., Di Leva, F.S., Brancaccio, D., Tomassi, S., Giuntini, S., Cerofolini, L., Fragai, M., Luchinat, C., Reichart, F., Cavallini, C., Costa, B., Piccarducci, R., Taliani, S., Da Settimo, F., Martini, C., Kessler, H., Novellino, E., Marinelli, L., 2018. Simultaneous Targeting of RGD-Integrins and Dual Murine Double Minute Proteins in Glioblastoma Multiforme. J. Med. Chem. 61, 4791–4809. https://doi.org/10.1021/acs.jmedchem.8b00004

Miyazaki, T., Uemae, Y., Ishikawa, E., 2017. CXCL12/CXCR4 signaling in glioma stem cells—prospects for therapeutic intervention. Translational Cancer Research 6, S434-S437–S437. https://doi.org/10.21037/12833

Moskovits, N., Kalinkovich, A., Bar, J., Lapidot, T., Oren, M., 2006. p53 Attenuates Cancer Cell Migration and Invasion through Repression of SDF-1/CXCL12 Expression in Stromal Fibroblasts. Cancer Res 66, 10671–10676. https://doi.org/10.1158/0008-5472.CAN-06-2323

Nimmagadda, S., Pullambhatla, M., Pomper, M.G., 2009. Immunoimaging of CXCR4 expression in brain tumor xenografts using SPECT/CT. J. Nucl. Med. 50, 1124–1130. https://doi.org/10.2967/jnumed.108.061325

Niu, J., Huang, Y., Zhang, L., 2015. CXCR4 silencing inhibits invasion and migration of human laryngeal cancer Hep-2 cells. Int J Clin Exp Pathol 8, 6255–6261.

Nuti, E., Casalini, F., Santamaria, S., Gabelloni, P., Bendinelli, S., Da Pozzo, E., Costa, B., Marinelli, L., La Pietra, V., Novellino, E., Margarida Bernardo, M., Fridman, R., Da Settimo, F., Martini, C., Rossello, A., 2011. Synthesis and biological evaluation in U87MG glioma cells of (ethynylthiophene)sulfonamido-based hydroxamates as matrix metalloproteinase inhibitors. European Journal of Medicinal Chemistry 46, 2617–2629. https://doi.org/10.1016/j.ejmech.2011.03.033

Ostrom, Q.T., Gittleman, H., Farah, P., Ondracek, A., Chen, Y., Wolinsky, Y., Stroup, N.E., Kruchko, C., Barnholtz-Sloan, J.S., 2013. CBTRUS statistical report: Primary brain and central nervous system tumors diagnosed in the United States in 2006-2010. Neuro-oncology 15 Suppl 2, ii1-56. https://doi.org/10.1093/neuonc/not151

Phillips, J.C., Braun, R., Wang, W., Gumbart, J., Tajkhorshid, E., Villa, E., Chipot, C., Skeel, R.D., Kalé, L., Schulten, K., 2005. Scalable molecular dynamics with NAMD. J Comput Chem 26, 1781–1802. https://doi.org/10.1002/jcc.20289

Popowicz, G.M., Czarna, A., Wolf, S., Wang, K., Wang, W., Dömling, A., Holak, T.A., 2010. Structures of low molecular weight inhibitors bound to MDMX and MDM2 reveal new approaches for p53-MDMX/MDM2 antagonist drug discovery. Cell Cycle 9, 1104–1111. https://doi.org/10.4161/cc.9.6.10956

Presti, M., Mazzon, E., Basile, M.S., Petralia, M.C., Bramanti, A., Colletti, G., Bramanti, P., Nicoletti, F., Fagone, P., 2018. Overexpression of macrophage migration inhibitory factor and functionally-related genes, D-DT, CD74, CD44, CXCR2 and CXCR4, in glioblastoma. Oncol Lett 16, 2881–2886. https://doi.org/10.3892/ol.2018.8990

Sestito, S., Daniele, S., Nesi, G., Zappelli, E., Di Maio, D., Marinelli, L., Digiacomo, M., Lapucci, A., Martini, C., Novellino, E., Rapposelli, S., 2016. Locking PDK1 in DFG-out conformation through 2-oxo-indole containing molecules: Another tools to fight glioblastoma. Eur J Med Chem 118, 47–63. https://doi.org/10.1016/j.ejmech.2016.04.003

Sestito, S., Runfola, M., Tonelli, M., Chiellini, G., Rapposelli, S., 2018. New Multitarget Approaches in the War Against Glioblastoma: A Mini-Perspective. Front Pharmacol 9. https://doi.org/10.3389/fphar.2018.00874

Shelley, J.C., Cholleti, A., Frye, L.L., Greenwood, J.R., Timlin, M.R., Uchimaya, M., 2007. Epik: a software program for pK(a) prediction and protonation state generation for drug-like molecules. J. Comput. Aided Mol. Des. 21, 681–691. https://doi.org/10.1007/s10822-007-9133-z

Uhrinova, S., Uhrin, D., Powers, H., Watt, K., Zheleva, D., Fischer, P., McInnes, C., Barlow, P.N., 2005. Structure of free MDM2 N-terminal domain reveals conformational adjustments that accompany p53-binding. J. Mol. Biol. 350, 587–598. https://doi.org/10.1016/j.jmb.2005.05.010

Wang, C.-L., Wang, J.-Y., Liu, Z.-Y., Ma, X.-M., Wang, X.-W., Jin, H., Zhang, X.-P., Fu, D., Hou, L.-J., Lu, Y.-C., 2014. Ubiquitin-specific protease 2a stabilizes MDM4 and facilitates the p53-mediated intrinsic apoptotic pathway in glioblastoma. Carcinogenesis 35, 1500–1509. https://doi.org/10.1093/carcin/bgu015

Wang, J., Wolf, R.M., Caldwell, J.W., Kollman, P.A., Case, D.A., 2004. Development and testing of a general amber force field. J Comput Chem 25, 1157–1174. https://doi.org/10.1002/jcc.20035

Werfel, T.A., Elion, D.L., Rahman, B., Hicks, D.J., Sanchez, V., Gonzalez-Ericsson, P.I., Nixon, M.J., James, J.L., Balko, J.M., Scherle, P., Koblish, H.K., Cook, R.S., 2018. Treatment-induced tumor cell apoptosis and secondary necrosis drive tumor progression in the residual tumor microenvironment through MerTK and IDO-1. Cancer Res. https://doi.org/10.1158/0008-5472.CAN-18-1106

Yu, J., Guo, M., Wang, T., Li, X., Wang, D., Wang, X., Zhang, Q., Wang, L., Zhang, Y., Zhao, C., Feng, B., 2016. Inhibition of cell proliferation, migration and invasion by a glioma-targeted fusion protein combining the p53 C terminus and MDM2-binding domain. Cell Prolif. 49, 79–89. https://doi.org/10.1111/cpr.12238

Zagzag, D., Lukyanov, Y., Lan, L., Ali, M.A., Esencay, M., Mendez, O., Yee, H., Voura, E.B., Newcomb, E.W., 2006. Hypoxia-inducible factor 1 and VEGF upregulate CXCR4 in glioblastoma: implications for angiogenesis and glioma cell invasion. Lab. Invest. 86, 1221–1232. https://doi.org/10.1038/labinvest.3700482

Zhang, Y., Dube, C., Gibert, M., Cruickshanks, N., Wang, B., Coughlan, M., Yang, Y., Setiady, I., Deveau, C., Saoud, K., Grello, C., Oxford, M., Yuan, F., Abounader, R., 2018. The p53 Pathway in Glioblastoma. Cancers (Basel) 10. https://doi.org/10.3390/cancers10090297

Zhou, K.X., Xie, L.H., Peng, X., Guo, Q.M., Wu, Q.Y., Wang, W.H., Zhang, G.L., Wu, J.F., Zhang, G.J., Du, C.W., 2018. CXCR4 antagonist AMD3100 enhances the response of MDA-MB-231 triple-negative breast cancer cells to ionizing radiation. Cancer Lett. 418, 196–203. https://doi.org/10.1016/j.canlet.2018.01.009